AGU ADVANCING EARTH AND SPACE SCIENCE

JAMES | Journal of Advances in Modeling Earth Systems®

RESEARCH ARTICLE
10.1029/2022MS003563

Global Surface Ocean Acidification Indicators From 1750 to 2100

Li-Qing Jiang[1,2], John Dunne[3], Brendan R. Carter[4,5], Jerry F. Tjiputra[6], Jens Terhaar[7,8,9], Jonathan D. Sharp[4,5], Are Olsen[10], Simone Alin[5], Dorothee C. E. Bakker[11], Richard A. Feely[5], Jean-Pierre Gattuso[12,13], Patrick Hogan[14], Tatiana Ilyina[15], Nico Lange[16], Siv K. Lauvset[6], Ernie R. Lewis[17], Tomas Lovato[18], Julien Palmieri[19], Yeray Santana-Falcón[20], Jörg Schwinger[6], Roland Séférian[20], Gary Strand[21], Neil Swart[22], Toste Tanhua[16], Hiroyuki Tsujino[23], Rik Wanninkhof[24], Michio Watanabe[25,26], Akitomo Yamamoto[25,26], and Tilo Ziehn[27]

[1]Cooperative Institute for Satellite Earth System Studies, Earth System Science Interdisciplinary Center, University of Maryland, College Park, MD, USA, [2]NOAA/NESDIS National Centers for Environmental Information, Silver Spring, MD, USA, [3]NOAA/OAR Geophysical Fluid Dynamics Laboratory, Princeton, NJ, USA, [4]Cooperative Institute for Climate, Ocean, and Ecosystem Studies, University of Washington, Seattle, WA, USA, [5]NOAA/OAR Pacific Marine Environmental Laboratory, Seattle, WA, USA, [6]NORCE Norwegian Research Centre, Bjerknes Centre for Climate Research, Bergen, Norway, [7]Department of Marine Chemistry and Geochemistry, Woods Hole Oceanographic Institution, Woods Hole, MA, USA, [8]Climate and Environmental Physics, Physics Institute, University of Bern, Bern, Switzerland, [9]Oeschger Centre for Climate Change Research, University of Bern, Bern, Switzerland, [10]Geophysical Institute, University of Bergen and Bjerknes Centre for Climate Research, Bergen, Norway, [11]Centre for Ocean and Atmospheric Sciences, School of Environmental Sciences, University of East Anglia, Norwich, UK, [12]Sorbonne Université, CNRS, Laboratoire d'Océanographie de Villefranche, Villefranche-sur-Mer, France, [13]Institute for Sustainable Development and International Relations, Paris, France, [14]NOAA/NESDIS National Centers for Environmental Information, Stennis Space Center, MS, USA, [15]Max Planck Institute for Meteorology, Hamburg, Germany, [16]GEOMAR Helmholtz Centre for Ocean Research Kiel, Kiel, Germany, [17]Brookhaven National Laboratory, Upton, NY, USA, [18]Ocean Modeling and Data Assimilation Division, Fondazione Centro Euro-Mediterraneo sui Cambiamenti Climatici, CMCC, Bologna, Italy, [19]National Oceanography Centre, European Way, Southampton, UK, [20]CNRM (Université de Toulouse, Météo-France, CNRS), Toulouse Cedex 1, France, [21]US National Center for Atmospheric Research, Boulder, CO, USA, [22]Canadian Centre for Climate Modelling and Analysis, University of Victoria, Victoria, BC, Canada, [23]JMA Meteorological Research Institute, Tsukuba, Japan, [24]NOAA/OAR Atlantic Oceanographic and Meteorological Laboratory, Miami, FL, USA, [25]Research Institute for Global Change, Japan Agency for Marine-Earth Science and Technology (JAMSTEC), Kanagawa, Japan, [26]Atmosphere and Ocean Research Institute, University of Tokyo, Chiba, Japan, [27]CSIRO Oceans and Atmosphere, Aspendale, VIC, Australia

Key Points:

- This study presents the evolution of 10 ocean acidification (OA) indicators in the global surface ocean from 1750 to 2100
- By leveraging 14 Earth System Models (ESMs) and the latest observational data, it represents a significant advancement in OA projections
- This inter-model comparison effort showcases the overall agreements among different ESMs in projecting surface ocean carbon variables

Supporting Information:

Supporting Information may be found in the online version of this article.

Correspondence to:

L.-Q. Jiang,
Liqing.Jiang@noaa.gov

Citation:

Jiang, L.-Q., Dunne, J., Carter, B. R., Tjiputra, J. F., Terhaar, J., Sharp, J. D., et al. (2023). Global surface ocean acidification indicators from 1750 to 2100. *Journal of Advances in Modeling Earth Systems*, *15*, e2022MS003563. https://doi.org/10.1029/2022MS003563

Received 14 FEB 2023
Accepted 3 MAR 2023

Abstract

Accurately predicting future ocean acidification (OA) conditions is crucial for advancing OA research at regional and global scales, and guiding society's mitigation and adaptation efforts. This study presents a new model-data fusion product covering 10 global surface OA indicators based on 14 Earth System Models (ESMs) from the Coupled Model Intercomparison Project Phase 6 (CMIP6), along with three recent observational ocean carbon data products. The indicators include fugacity of carbon dioxide, pH on total scale, total hydrogen ion content, free hydrogen ion content, carbonate ion content, aragonite saturation state, calcite saturation state, Revelle Factor, total dissolved inorganic carbon content, and total alkalinity content. The evolution of these OA indicators is presented on a global surface ocean 1° × 1° grid as decadal averages every 10 years from preindustrial conditions (1750), through historical conditions (1850–2010), and to five future Shared Socioeconomic Pathways (2020–2100): SSP1-1.9, SSP1-2.6, SSP2-4.5, SSP3-7.0, and SSP5-8.5. These OA trajectories represent an improvement over previous OA data products with respect to data quantity, spatial and temporal coverage, diversity of the underlying data and model simulations, and the provided SSPs. The generated data product offers a state-of-the-art research and management tool for the 21st century under the combined stressors of global climate change and ocean acidification. The gridded data product is available in NetCDF at the National Oceanic and Atmospheric Administration (NOAA) National Centers for Environmental Information: https://www.ncei.noaa.gov/data/oceans/ncei/ocads/metadata/0259391.html, and global maps of these indicators are available in jpeg at: https://www.ncei.noaa.gov/access/ocean-carbon-acidification-data-system/synthesis/surface-oa-indicators.html.

Plain Language Summary

A new data product, based on the latest computer simulations and observational data, offers improved projections of ocean acidification (OA) conditions from the start of the Industrial Revolution in 1750 to the end of the 21st century. These projections will support OA research at

regional and global scales, and provide essential information to guide OA mitigation and adaptation efforts for various sectors, including fisheries, aquaculture, tourism, marine resource decision-makers, and the general public.

1. Introduction

Since the beginning of global industrialization, the ocean has taken up 20%–30% of all anthropogenic carbon dioxide (CO_2) emitted from fossil fuel combustion, cement production, and land use change (Friedlingstein et al., 2022; Gruber et al., 2019, 2023; Sabine et al., 2004; Terhaar, Frölicher, & Joos, 2022). Without ocean uptake, the atmospheric CO_2 (dry-air mixing ratio) would be ∼80 parts per million (ppm) greater than its current value of 419 ppm (2022 annual average, Tans & Keeling, 2023). The ocean is thus slowing down the rise of anthropogenic CO_2, a major contributor to global climate change (Friedlingstein et al., 2022; IPCC, 2021; IPCC, 2022).

The anthropogenic carbon dioxide taken up by the ocean alters the ocean's carbonate chemistry (DeVries, 2022). The mildly alkaline ocean is acidifying, and its carbonate ion content ($[CO_3^{2-}]$, a building block for calcifying marine organisms) is decreasing in a process commonly referred to as "ocean acidification (OA)" (Caldeira & Wickett, 2003; Doney et al., 2009; Fabry et al., 2009; Feely et al., 2004; Gattuso & Hansson, 2011; Orr et al., 2005). OA is making it more difficult for marine calcifiers to build shells and skeletal structures from calcium carbonate ($CaCO_3$), thus negatively impacting their growth, reproduction, and survival rates (Fabry et al., 2009; Kroeker et al., 2013; Orr et al., 2005). These negative impacts on calcifying organisms are endangering coral reefs (Albright et al., 2016; Andersson & Gledhill, 2013) and broader marine ecosystems (Connell et al., 2018; Doney et al., 2020; Gattuso et al., 2015; Kawahata et al., 2019).

From 1750 to 2000, the average pH of the global surface ocean decreased by ∼0.11 units, equivalent to an acidity increase of ∼30% (Caldeira & Wickett, 2003; Jiang et al., 2019; Orr et al., 2005). From 2000 to 2100, this quantity is projected to decrease by 0.3–0.4 units (∼100%–150% increase in acidity) under the high-emission, low-mitigation SSP5-8.5 (Kwiatkowski et al., 2020). Such a profound and rapid change in ocean chemistry will likely jeopardize important ocean ecosystem goods and services—including food security, fisheries and aquaculture industry, recreational enterprises, and other Blue Economy-related activities—for billions of people.

While Earth System Models (ESMs) enable simulating and projecting changes for some ocean carbon variables, for example, partial pressure of carbon dioxide (pCO_2), total dissolved inorganic carbon content (DIC), and total alkalinity content (TA), they often suffer from model drift and may disagree in their ocean baseline conditions (Kwiatkowski et al., 2020; Steiner et al., 2014; Terhaar, Frölicher, & Joos, 2022). Observational data and control simulations can often improve ESM-based projections by providing more realistic baseline conditions and benchmarks for modeled changes, thus reducing model bias and drift (Orr et al., 2005; Séférian et al., 2016). Following the approach pioneered by Orr et al. (2005), Jiang et al. (2019) created a model-data fusion product by combining ∼23 million observations in the 6th version of the Surface Ocean CO_2 Atlas (SOCATv6, 1991–2018, Bakker et al., 2016) with a NOAA Geophysical Fluid Dynamic Laboratory (GFDL) Earth System Model, that is, GFDL-ESM2M (Dunne et al., 2013) to provide updated, expanded, and improved trends in pH on total scale (pH_T), total hydrogen ion content ($[H^+]_{total}$), and Revelle Factor (RF, a measure of the ocean's buffer capacity) at all locations of the global surface ocean from 1850 to 2100.

Since the publication of the Jiang et al. (2019) product, observational data products, for example, a more recent version of the SOCAT (version 2022, Bakker et al., 2016), the Global Ocean Data Analysis Project version 2 (GLODAPv2, version 2022, Lauvset et al., 2022), and the Coastal Ocean Data Analysis Product in North America (CODAP-NA, version 2021, Jiang et al., 2021), along with the next generation of ESMs, that is, those participating in the Coupled Model Intercomparison Project Phase 6 (CMIP6), have been made public. From CMIP5 to CMIP6, modeling centers have further developed their models, increased the models' resolutions, and implemented more processes explicitly (Eyring et al., 2016; Séférian et al., 2020). For example, GFDL's 2nd generation Earth System Model (ESM2M) with a horizontal resolution of $1° \times 1°$ in the ocean and no explicit representation of sediment processes has now been replaced with its successors: GFDL-ESM4.1 with a horizontal resolution of $0.5° \times 0.5°$ (Dunne, Horowitz, et al., 2020; Stock et al., 2020), and GFDL-CM4.0 with a horizontal resolution of $0.25° \times 0.25°$ (Dunne, Bociu, et al., 2020; Held et al., 2019), both of which now include an explicit representation of ocean sedimentation processes. The CMIP6 ESMs also have a higher equilibrium climate sensitivity (ECS), on average, than the CMIP5 ones (Nijsse et al., 2020; Tokarska et al., 2020; Zelinka et al., 2020). Compared to Jiang

Table 1
Shared Socioeconomic Pathways (SSPs) Based on Meinshausen et al. (2020)

SSP	Projected values in 2100			Description
	Atmospheric CO_2 (ppm)	Surface air temperature increase (°C)	Radiative forcing ($W\,m^{-2}$)	
SSP1-1.9	393	1.1 (0.6–1.8)	1.9	"Low-emission, high-mitigation scenario" that reflects most closely a 1.5°C target under the Paris Agreement
SSP1-2.6	446	1.6 (0.9–2.4)	2.6	"2°C scenario" of the "sustainability" SSP1 socioeconomic family
SSP2-4.5	603	2.8 (1.8–4.1)	4.5	"Middle of the road scenario" of the SSP2 socioeconomic family
SSP3-7.0	867	4.4 (3.0–6.5)	7.0	"Medium-high emission scenario" within the "regional rivalry" socioeconomic family
SSP5-8.5	1135	5.8 (3.8–8.6)	8.5	"High-emission, low-mitigation scenario" that reflects fossil-fuel based management and a high end of the range of future pathways

et al. (2019), who used only one CMIP5 model, that is, GFDL-ESM2M (Dunne et al., 2013; Taylor et al., 2012), the present analysis used outputs from 14 CMIP6 models to reduce potential projection biases in OA indicators that are more likely in single ESMs than across an entire ensemble (Terhaar et al., 2020, 2021a).

Not only have the participating ESMs changed from CMIP5 to CMIP6, but also the concentration pathways. The IPCC's AR6 (Working Group I) has now adopted the new Shared Socioeconomic Pathways (SSP1-1.9, SSP1-2.6, SSP2-4.5, SSP3-7.0, and SSP5-8.5) (Table 1) (Meinshausen et al., 2020; O'Neil et al., 2014; O'Neill et al., 2016; Riahi et al., 2017), in place of the previous Representative Concentrations Pathways (RCP2.6, RCP4.5, RCP6.0, and RCP8.5) (Meinshausen et al., 2011; Riahi et al., 2011; van Vuuren et al., 2011) [used by Jiang et al. (2019)], which themselves replaced the IS92 emission scenarios (IS92a, IS92b, IS92c, IS92d, IS92e, IS92f) (IPCC, 2000) [used by Orr et al. (2005)]. These SSPs converge approximately to the same radiative forcing in 2100 as the RCPs (indicated by the last two digits, e.g., 8.5 for 8.5 W m^{-2}), but differ in the concentration levels of the various greenhouse gases and forcing agents, such as aerosols. For example, SSP5-8.5 assumes more CO_2 emissions and fewer emissions of other greenhouse gases over the 21st century than RCP8.5, so that the atmospheric CO_2 levels of SSP5-8.5 in 2100 are around 200 ppm higher than in RCP8.5 (Meinshausen et al., 2020).

Compared to Jiang et al. (2019), the present study also considers changes in other parameters besides DIC and temperature. For example, salinity changes due to climate change are already detectable (Durack et al., 2012; Zika et al., 2018) and may influence projections of OA indicators by reducing TA regionally, for example, in the Arctic Ocean (Terhaar, Torres, et al., 2021). While TA changes attributable to long-term climate feedbacks are difficult to detect globally at present (Carter et al., 2016; Ilyina et al., 2009), they can already be observed in some regions, for example, the Arctic (Drake et al., 2018; Woosley & Millero, 2020). TA redistribution from OA feedbacks may or may not be detectable by the end of the current century (i.e., 2100)—and the CMIP6 models differ in their parameterizations of these processes—but freshwater cycle changes alone would be expected to change regional TA distribution and OA by that time (Terhaar, Torres, et al., 2021).

In the present study, 10 surface OA indicators, that is, fCO_2, pH on total scale (pH_T), total hydrogen ion content ($[H^+]_{total}$), free hydrogen ion content ($[H^+]_{free}$), carbonate ion content ($[CO_3^{2-}]$, aragonite saturation state (Ω_{arag}), calcite saturation state (Ω_{calc}), Revelle Factor (RF), DIC, and TA, are calculated on a global surface ocean 1° × 1° grid as decadal averages every 10 years in 1750 and all decades from 1850 to 2100 based on the latest projections from 14 CMIP6 ESMs, together with three recent observational data products: the Surface Ocean CO_2 Atlas (SOCAT, version 2022, Bakker et al., 2016), the Global Ocean Data Analysis Project Version 2 (GLODAPv2, version 2022, Lauvset et al., 2022), and the Coastal Ocean Data Analysis Product in North America (CODAP-NA, version 2021, Jiang et al., 2021). The resultant projections of global surface ocean OA indicators provide a state-of-the-art research and management tool for the 21st century under the combined global stressors of ocean warming and acidification.

2. Methods

A model-data fusion product was created by applying adjustments to the outputs of 14 CMIP6 ESMs with the latest observational data in the steps below:

1. Sea surface temperature (SST), sea surface salinity (SSS), DIC, and TA were extracted or calculated from SOCAT (version 2022), GLODAPv2 (version 2022), and CODAP-NA (version 2021). The temporally adjusted DIC (to the year of 2010), as well as SST, SSS, and TA were interpolated onto a global surface ocean $1° \times 1°$ grid.
2. Proxy-based DIC and TA calculated with gridded temperature, salinity, and dissolved oxygen content (DO) from the World Ocean Atlas (WOA-2018) were used to further quality control (QC) the gridded observational DIC and TA data, especially in data-sparse regions.
3. The temporal evolution (decadal averages of every 10 years) of global SST, SSS, DIC, and TA from 1850 to 2100 out of 14 ESMs was adjusted with offsets that were derived based on the differences between the model output in 2010 and the corresponding observational data in 2010 at that grid point (see Section 2.4 for more details).
4. The adjusted trajectories of SST, SSS, DIC, and TA from these ESMs, as well as constant phosphate and silicate content from WOA-2018, were used to calculate all surface OA indicators at all locations of the global surface ocean grid in all decades from 1850 to 2100.
5. OA indicators in 1750 were approximated by assuming that sea surface fCO_2 increased at the same rate as atmospheric CO_2 levels from 1750 to 1850, while SST, SSS, and TA remained at their levels in 1850.

2.1. Observational Data

The latest observational ocean carbon data from SOCAT (version 2022, 1957–2021, 33.7 million surface-only fCO_2 observations, Bakker et al., 2016), GLODAPv2 (version 2022, 1972–2021, 1.4 million discrete bottle-based surface and subsurface observations, Lauvset et al., 2022), and CODAP-NA (version 2021, 2003–2018, 3,391 discrete bottle-based surface and subsurface observations, Jiang et al., 2021) were used for this analysis. SOCAT provides the best temporal and spatial coverage, but has only one ocean carbon parameter: fCO_2. Only SOCAT data with a World Ocean Circulation Experiment (WOCE) QC flag of 2 (good data) and a cruise flag of A, B, C, and D (fCO_2 accuracy $\leq$5 µatm) were used for this analysis (Bakker et al., 2016). TA, phosphate content, and silicate content, which are required to calculate the rest of the OA indicators, were estimated using the Empirical Seawater Property Estimation Routines (ESPER) from SST and SSS (Carter et al., 2021). ESPER is an empirical algorithm that is trained with global surface and interior ocean variables. It allows a user to estimate DIC, TA, and several other seawater properties from input variables, such as salinity (minimally required), temperature, and dissolved oxygen (DO), along with longitude, latitude, and depth. GLODAPv2 and CODAP-NA have substantially sparser spatial coverage than SOCAT, but offer additional ocean carbon variables. Only data from these products with at least a pair of DIC and TA, DIC and pH, or TA and pH, and a sampling depth of $\leq$20 m were used for this analysis. If DIC, TA, and pH were all available, DIC and TA were used.

In all observational data products, DIC was adjusted to 2010 using ESPER. Two sets of ESPER calculations were conducted based on input variables of temperature, salinity, longitude, latitude, and depth: one with the atmospheric CO_2 dry-air mixing ratio at the sampling time and another one with the atmospheric CO_2 dry-air mixing ratio at 2010. The difference in the output DIC between the two sets of ESPER calculations was assumed to be the temporal DIC change due to the ocean's absorption of anthropogenic CO_2 from the sampling year to 2010. This difference was then used to adjust DIC to the year of 2010. The CO_2 system calculation was performed using a Julia version of the CO2SYS (CO2System.jl, v2.0.5, https://github.com/mvdh7/CO2System.jl, Humphreys et al., 2022) with the dissociation constants and parameters as recommended by Jiang et al. (2022), that is, dissociation constants for carbonic acid of Lueker et al. (2000), bisulfate (HSO_4^-) of Dickson (1990), hydrofluoric acid (HF) of Perez and Fraga (1987), and the total borate content of Lee et al. (2010).

DIC adjusted to 2010, as well as SST, SSS, and TA from these three data products were then pooled as one observational database that was interpolated onto a global surface ocean $1° \times 1°$ grid. This product is primarily based on SOCAT due to its much larger data quantity. 19,193,038 data points (or 99.8% of the total) compared to only 44,165 data points (0.2%) from the GLODAPv2 and CODAP-NA combined. That said, data points from GLODAPv2 and CODAP-NA play an unproportionally important role in filling up some data sparse regions (see

Figure 1 of Feely et al., 2023). Interpolation and gap-filling was done with a Julia version of the Data-Interpolating Variational Analysis (DIVAnd.jl, https://github.com/gher-ulg/DIVAnd.jl, Barth et al., 2014). The correlation lengths of 21° latitudinally and 42° longitudinally, as well as the noise to signal ratio of 0.1, were selected to strike a balance between retaining some regional variability and smoothing over fine scale variability that is present in synoptic measurements but not representative of climatological conditions (see also Jiang et al., 2019).

2.2. Proxy-Based DIC and TA

Proxy-based DIC and TA values, calculated with the gridded (1° × 1°) SST, SSS, and DO data (average of all values from 1981 to 2010, or "Climate Normal") out of the World Ocean Atlas 2018 (Garcia et al., 2019) using the ESPER algorithms (Carter et al., 2021), were used to help establish a climatological state to identify unrealistic values, anomalies, and outliers. Specifically, these proxy-based data were used to QC the gridded cruise-based observational DIC and TA data, primarily by identifying "bullseyes" on the interpolated maps, and blanking out regions with large differences between gridded values and the corresponding proxy-based values but little observational coverage (Tables S1 and S2 in Supporting Information S1).

2.3. Model Output

All CMIP6 ESMs use the new Shared Socioeconomic Pathways, for example, SSP1-1.9, SSP1-2.6, SSP2-4.5, SSP3-7.0, SSP5-8.5, to simulate future societal choices in terms of greenhouse gas emissions (Meinshausen et al., 2020; O'Neil et al., 2014; Riahi et al., 2017). 18 CMIP6 ESMs provided ocean surface temperature (tos), surface salinity (sos), dissolved inorganic carbon (dissic), and total alkalinity (talk). These 18 ESMs used 14 distinctive ocean biogeochemical models (Table S3 in Supporting Information S1). To avoid giving too much weight to the same ocean biogeochemical models that were used among different ESMs, only 14 ESMs were used in this study. These ESMs return output variables following Climate and Forecast convention designations for tos, sos, dissic, and talk (Hassell et al., 2017). Their outputs were used to reconstruct and project the temporal changes from 1850 to 2100. Note that not all of these ESMs provide output for all five SSPs (Table 1).

These ESMs provide dissic and talk output in mol m^{-3}. Both variables were converted to content in μmol kg^{-1} using either the simulated density at each grid point and each timestep or a model-specific density conversion factor for ESMs that did not use a spatially and temporally varying densities for conversion (Table S3 in Supporting Information S1). The density at each grid point of a timestamp was calculated from model output of SST, SSS, and latitude using the Thermodynamic Equation of Seawater—2010 (TEOS-10, http://www.teos-10.org) (IOC et al., 2010; McDougall & Barker, 2011).

To minimize the influences of modeled interannual variability in any particular year, all 10 years of model results for each decade were averaged to calculate a single value for that decade. For example, SST, SSS, DIC, and TA at each grid point of the global surface ocean in the decade of 2010 were calculated as the mean of all values at that location from January 2005 to December 2014. Outputs from models that were not originally on a 1° × 1° grid were re-gridded onto the same 1° × 1° grid using the DIVA tool with the same correlation lengths as mentioned above.

2.4. Bias and Drift Adjustments

Two adjustments were made to SST, SSS, DIC, and TA: one to remove model biases using observational data, and one to remove model drift using preindustrial control (piControl). The model biases were removed by subtracting from the modeled values the difference of the respective 2010 model output at a particular grid point and the corresponding observational value at the same location in the same decade. The same offset adjustment (absolute value) is then applied to all periods from 1850 to 2100 at that grid point.

In addition, the model drift was removed for DIC and TA using their corresponding piControl values. Similar to other variables, the piControl values were averaged over a 10-year period to remove interannual variabilities. The piControl start points were determined using the "parent_time_units" and "branch_time_in_parent" values stored in the "historical" model output file. For example, a "parent_time_units" of "days since 1850-01-01" and a "branch_time_in_parent" of "124,183 days" (340 years) would mean that the piControl start point for that historical variant is 1850 + 340 = 2190; that is, a piControl value of 1 January 2190 corresponds to the Gregorian

calendar date of 1 January 1850 for that variant of the model. Start points of different ESMs are listed in Table S3 in Supporting Information S1).

The model bias and drift adjustments were conducted at each grid point using Equation 1:

$$\mathrm{DIC}[i] = \mathrm{DIC}[2010] + [(\mathrm{dissic}[i] - \mathrm{dissic\_pi}[i]) - (\mathrm{dissic}[2010] - \mathrm{dissic\_pi}[2010])] \quad (1)$$

where DIC[i] is the adjusted DIC in the decade around year i (decadal mean) on a particular grid point; DIC[2010] is the observation-based DIC at the same location in 2010 (decadal mean); dissic[i] and dissic[2010] are the model-based DIC at that same location in the decade around year i (decadal mean) and 2010 (decadal mean), respectively; and dissic_pi[i] and dissic_pi[2010] are the piControl simulation DIC corresponding to the decades around year i (decadal mean) and 2010 (decadal mean), respectively.

The adjusted SST, SSS, DIC, and TA at a grid point in a particular decade were then used to calculate the rest of the OA indicators using CO2System.jl (Humphreys et al., 2022) with the set of constants described in Section 2.1. As some ESMs do not simulate silicate and phosphate contents, for consistency purposes, gridded values of both nutrient contents were derived from observations, that is, WOA-2018 ("Climate Normal", Garcia et al., 2019) and assumed to be constant over time. While absolute values of OA indicators are sensitive to these inputs, these sensitivities are sufficiently small that the omission of temporal trends in these inputs is unlikely to be an important contributor to uncertainty in our data product (Orr et al., 2018).

2.5. Estimating OA Indicators in 1750

As most ESMs start their historical simulations at model year 1850, an approximation of OA indicators in 1750 is obtained using ice core-based atmospheric CO_2 data from 1752 (276.39ppm) and 1852 (288.57ppm) (Ethridge et al., 1996; MacFarling Meure et al., 2006). These data were used to approximate the oceanic fCO_2 change from 1750 to 1850 at all locations of the global ocean under the assumptions that SST, SSS, and TA were constant from 1750 to 1850. Similarly, the other OA indicators for 1750 were calculated using CO2System.jl with the recommended set of parameters described in Section 2.1.

2.6. DIC Versus fCO_2 as "Anchor" Variables

The results of this study are based on calculations using the bias- and drift-adjusted SST, SSS, DIC, and TA, and silicate and phosphate contents from WOA-2018 to calculate the OA indicators. However, such calculations could also be done with DIC and TA replaced by other ocean carbon variables. Because not all ESMs use the same equilibrium constants in their ocean biogeochemical model components, the choice of the input variables may affect the resulting OA indicators. An analysis in which DIC was replaced with fCO_2 yields similar results (Figure S1 in Supporting Information S1). In this manuscript, DIC was used instead of fCO_2 because it is available for more ESMs.

3. Results and Discussion

Unless otherwise noted, the results of this study are based on the bias-adjusted and drift-adjusted model output. Throughout the manuscript, the inter-model median values of the 14 ESMs and their standard deviations are provided. Median values were chosen instead of mean values to avoid the possibility that one outlier significantly skews a result. In addition, bias- and drift-adjusted model outputs for each of the individual ESMs are availabled in the published data product.

3.1. Comparison of Different Models

A comparison of SST, SSS, DIC, and TA (area-averaged globally), as well as the other OA indicators calculated based on these quantities, from all 14 ESMs are presented in Table S4 in Supporting Information S1 for 1850, 2010, and 2100. The inter-model standard deviations of the globally area-averaged SST, SSS, and sea surface DIC and TA in all decades from 1850 to 2100 are approximately 0.6°C (ranging between decades from 0.48 to 0.95°C), 0.17 (0.16–0.18), 42 μmol kg^{-1} (38–52 μmol kg^{-1}), and 49 μmol kg^{-1} (47–55 μmol kg^{-1}), respectively (Figure 1). The large variations across the model ensemble indicate that the models perform differently due to differences in their representations of processes, resolutions, and baseline conditions.

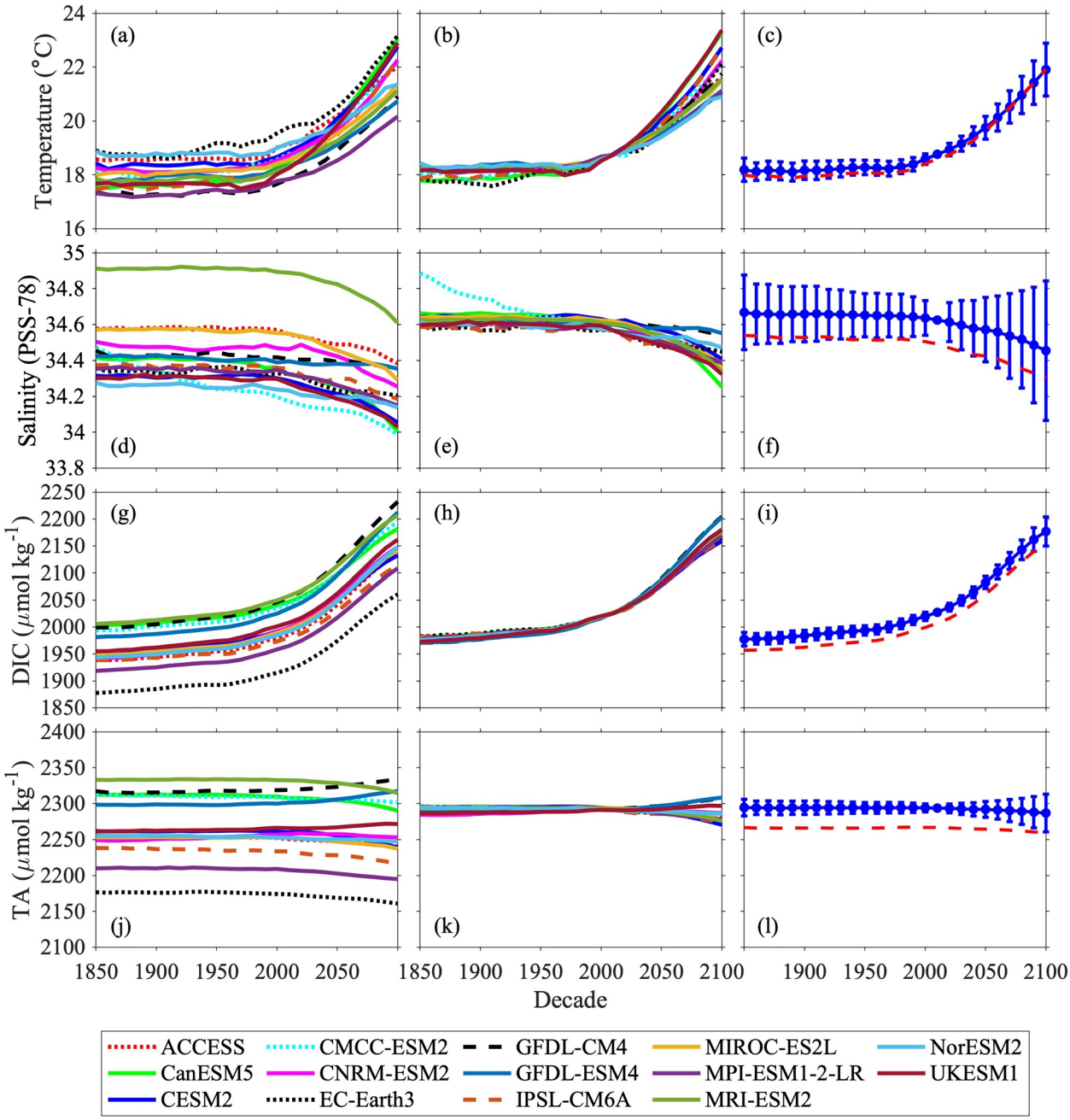

Figure 1. Temporal changes of suface ocean temperature, salinity, total dissolved inorganic carbon content (DIC), and total alkalinity content (TA) (area-averaged globally) from 1850 to 2100 under the historical and Shared Socioeconomic Pathway (SSP5-8.5). The four leftmost panels (a, d, g, and j) show raw model output. The four panels in the middle column (b, e, h, and k) show the results after applying the bias adjustment to the model output using observational data (drift-adjustment have been applied for DIC and TA). The four rightmost panels (c, f, i, and l) show the inter-model median values (dots) and 1σ ensemble spreads (error bars) after adjusting the model output with observational data (in blue) and the inter-model median values before the adjustment (dashed red lines).

3.2. Bias- and Drift-Adjusted Model Outputs

Our results show that adjusting model output with observational data reduces the inter-model differences of the OA indicators across all decades and not just in 2010 when the differences are forced to zero (Figure 1 and Figures S2 and S3 in Supporting Information S1). For example, the standard deviations of DIC are reduced from an average of 26 μmol kg^{-1} (ranging between decades from 25 to 34 μmol kg^{-1}) to an average of 4 μmol kg^{-1} (ranging from 0 in 2010 to 15 μmol kg^{-1}). Overall, the largest projection uncertainties of OA indicators come

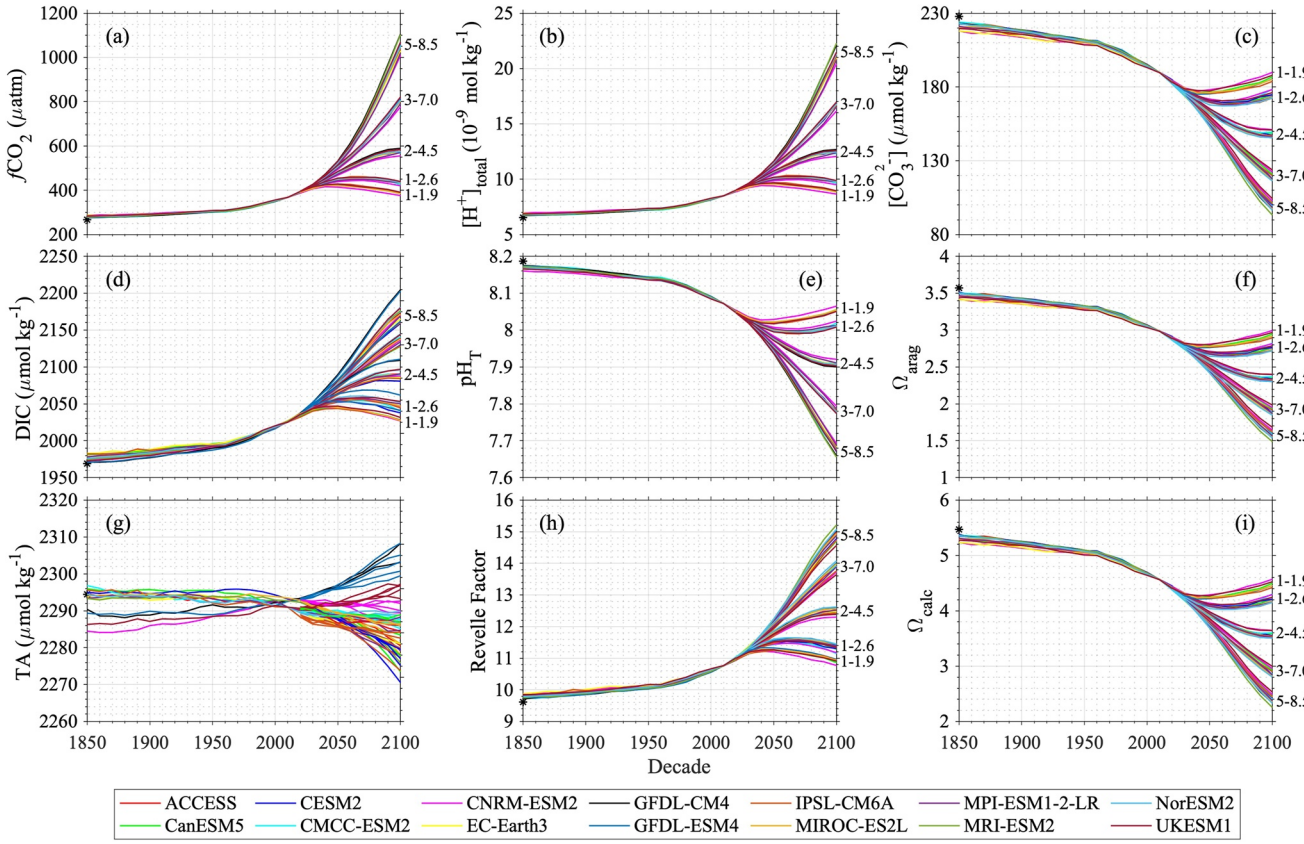

Figure 2. Temporal changes of global average surface ocean ocean acidification (OA) indicators as reconstructed and projected from 14 CMIP6 Earth System Models (Table S3 in Supporting Information S1) after applying adjustments with observational data: (a) fugacity of carbon dioxide (fCO_2), (b) total hydrogen ion content ($[H^+]_{total}$), (c) carbonate ion content ($[CO_3^{2-}]$), (d) total dissolved inorganic carbon content (DIC), (e) pH on total scale (pH_T), (f) aragonite saturation state (Ω_{arag}), (g) total alkalinity content (TA), (h) Revelle Factor (RF), and (i) calcite saturation state (Ω_{calc}). The asterisk signs on the left-side *y*-axes show the values in 1750. The numbers along right-side *y*-axes, that is, 1–1.9, 1–2.6, 2–4.5, 3–7.0, and 5–8.5, indicate the Shared Socioeconomic Pathways: SSP1-1.9, SSP1-2.6, SSP2-4.5, SSP3-7.0, and SSP5-8.5, respectively. These are missing from panel g because the trajectories were more dependent on the model than the SSPs.

from differences in the simulated pre-industrial state and not from changes over time (Figure 1). Whereas the sum of the processes simulated by ESMs provides the best estimates of changes in surface OA indicators over time, the observational fields represent the best estimates for the true values of those variables in 2010. So, in addition to enhancing consistency among individual models, adjusting model output with observational fields ensures that the magnitudes of the OA indicators reported here, either past reconstructions or future projections, converge as nearly as possible to their true values.

Overall, the adjustments forfCO_2, pH_T $[H^+]_{total}$, and $[H^+]_{free}$ are less than those for the rest of the OA indicators, for example, DIC, TA, $[CO_3^{2-}]$, calcium carbonate mineral saturation states, and RF (Figure 1 and Figures S2 and S3 in Supporting Information S1). ESMs tend to agree on surface seawater fCO_2, pH_T, $[H^+]_{total}$, and $[H^+]_{free}$ (Figure S2 in Supporting Information S1). Surface seawater fCO_2 is strongly controlled by its equilibrium with the atmosphere, which is prescribed in all ESMs by the same trajectories (Tjiputra et al., 2014). Furthermore, surface seawater fCO_2 is strongly correlated with $[H^+]_{total}$, $[H^+]_{free}$, and pH_T (Figure S4 in Supporting Information S1) (Caldeira & Berner, 1999). In comparison, DIC and TA are more biased (Figure 1), and biases in DIC are of similar magnitude and same direction as biases in TA, as the surface DIC adjusts during the spin-up via air-sea CO_2 flux to biases in TA, keeping fCO_2 close to its equilibrium with the atmosphere.

3.3. Global Surface OA Indicators in 1750 and From 1850 to 2100

Most OA indicators, including fCO_2, DIC, pH_T, $[H^+]_{total}$, $[H^+]_{free}$, $[CO_3^{2-}]$, Ω_{arag}, Ω_{calc}, and RF show large changes with time and rapid increases in their rates of change with time, especially under the high-emission scenarios of SSP3-7.0 and SSP5-8.5 (Figure 2–4 and Figure S5 in Supporting Information S1). In comparison, these

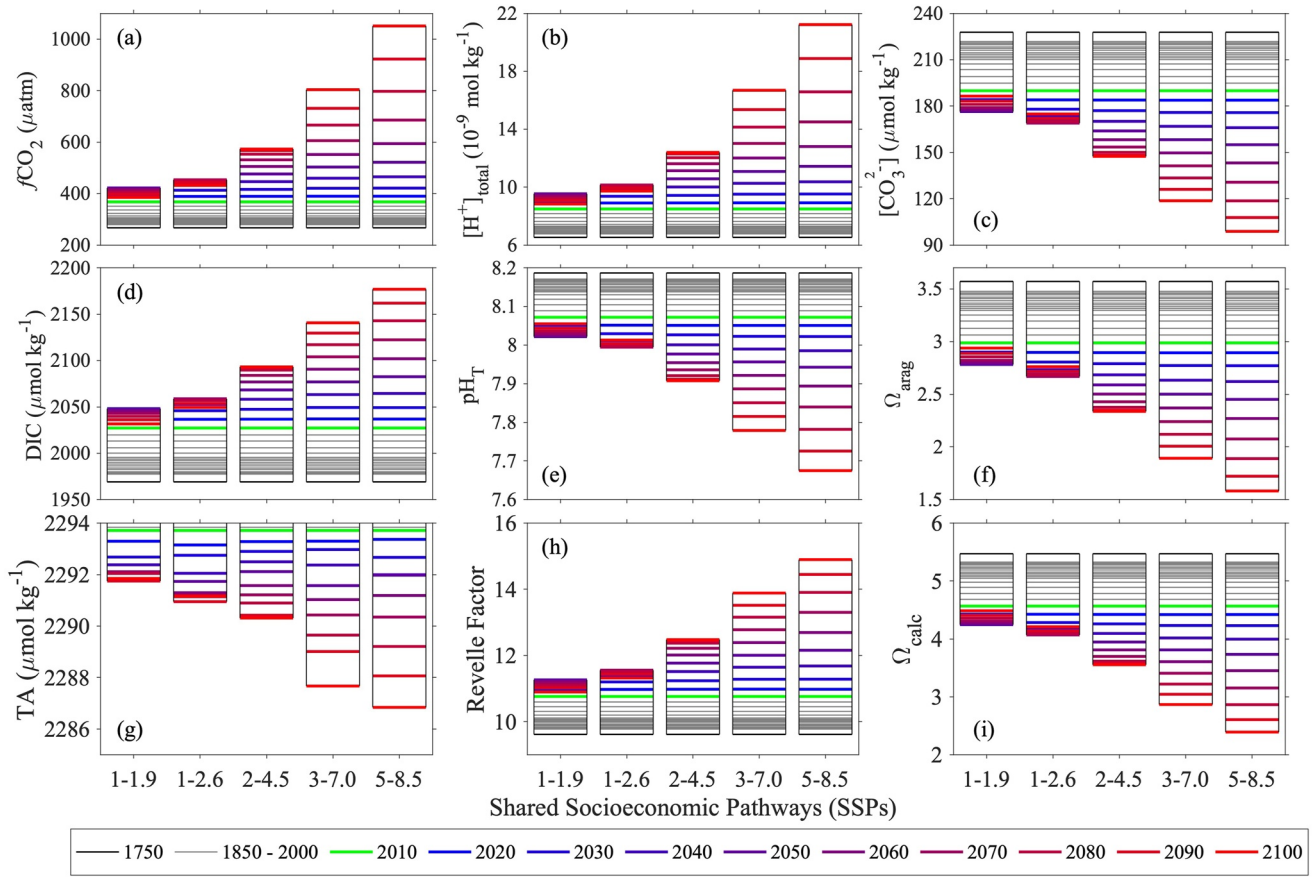

Figure 3. Temporal changes of global surface ocean acidification indicators (inter-model median values out of 14 CMIP6 Earth System Models after applying adjustments with observational data, area-averaged). Refer to Figure 2 for the full names of the variable abbreviations on the Y-axes. The *x*-axes labels, that is, 1–1.9, 1–2.6, 2–4.5, 3–7.0, and 5–8.5 indicate the Shared Socioeconomic Pathways: SSP1-1.9, SSP1-2.6, SSP2-4.5, SSP3-7.0, and SSP5-8.5, respectively.

OA indicators show only slight changes from current levels under the low-emission, high-mitigation SSP1-1.9 (Figure S6 in Supporting Information S1). Most models project an area-averaged TA change of <1% from 2010 to 2100. ESMs differ in how various biogeochemical model components simulate alkalinity fluxes from rivers and into sediments (Planchat et al., 2022; Séférian et al., 2019) and in how they parameterize feedbacks from OA on carbonate mineral cycling. For instance, the GFDL models allow for decreased surface ocean export of $CaCO_3$ with declining saturation states of aragonite and calcite from OA, which results in TA accumulation within the surface ocean in the later portions of the projections (Figure 2g). However, many models do not contain this potential feedback and therefore primarily exhibit TA trajectories dominated by dilution from increasing freshwater content with continued icemelt.

3.3.1. Fugacity of Carbon Dioxide (fCO_2)

Surface ocean fCO_2 is strongly controlled by air-sea CO_2 gas exchange (Broeker et al., 1979). Over the 100 years from 1750 to 1850, ice-core records suggest that the global area-averaged surface ocean fCO_2 increased by 12 µatm from 267 ppm µatm to 279 µatm (Tables S5 and S6 in Supporting Information S1). In the following 160 years from 1850 to 2010, the increase in surface ocean fCO_2 as estimated by ESMs was 89 µatm to reach 368 µatm (Tables S7 and S8 in Supporting Information S1). Over the 21st century, the global area-averaged surface ocean fCO_2 is projected to peak in 2050 at 422 µatm and to decrease to 385 µatm in 2100 under the low-emission, high mitigation SSP1-1.9. In comparison, if CO_2 emissions continue over the entire 21st century, the global area-averaged fCO_2 is projected to increase steadily to 573, 804, and 1051 µatm in 2100 under SSP2-4.5, SSP3-7.0, and SSP5-8.5, respectively (Tables S7 and S8 in Supporting Information S1; Figures 3 and 5).

Air-sea gas exchange tends to bring surface ocean fCO_2 close to equilibrium with the atmosphere, but disequilibria (e.g., due to sea-ice cover, or upwelling of high-fCO_2 water, or following biological drawdown of DIC or

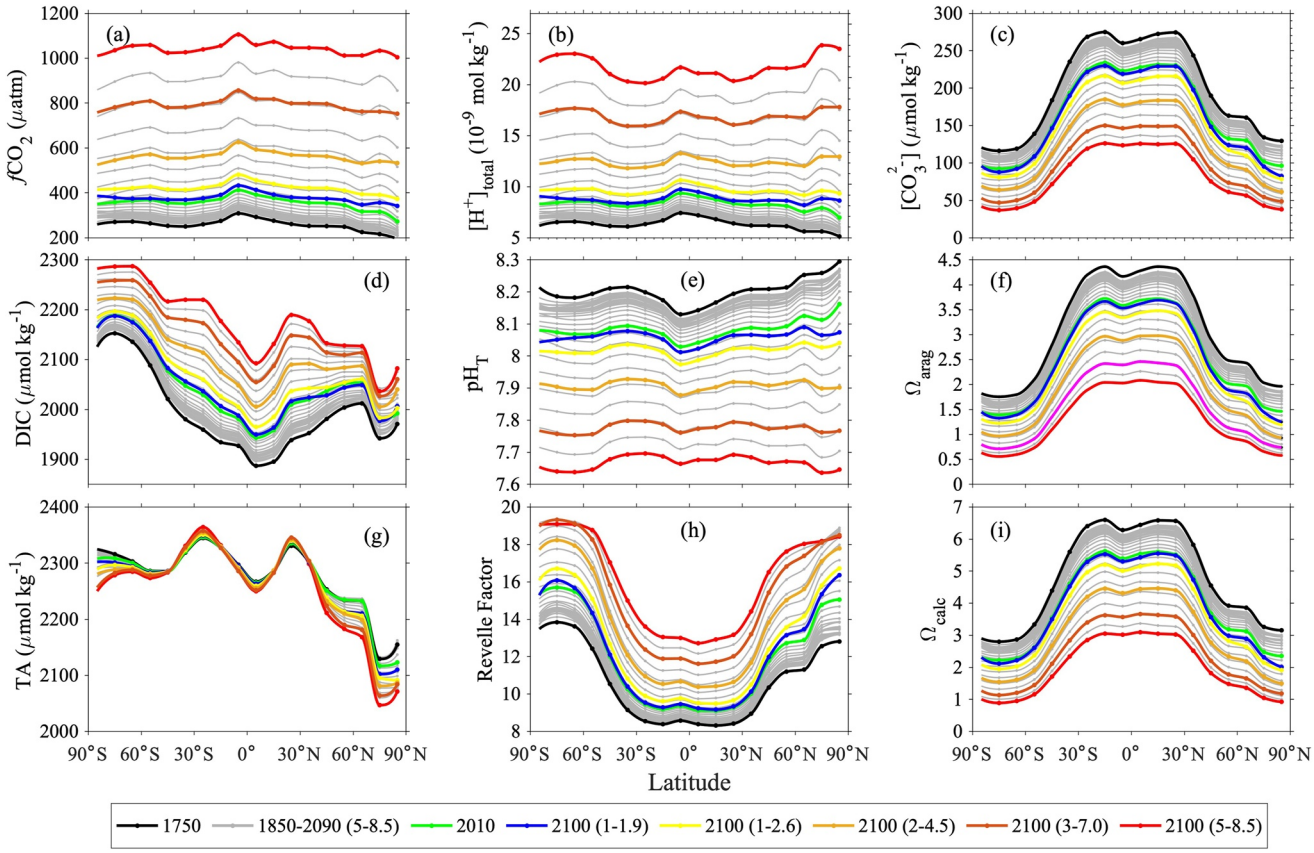

Figure 4. Decadal changes of global surface ocean acidification indicators along the latitudinal bands (inter-model median, area-averaged): 85°S (90°S to 80°S), 75°S (80°S to 70°S), …, 85°N (80°N to 90°N) from 1750 to 2100 under different Shared Socioeconomic Pathways (SSPs). Black dots and lines represent values in 1750. Green dots and lines represent values in 2010. The gray dots and lines are values from 1850 to 2000 under the historical simulation, and 2020 to 2090 under SSP5-8.5. Dots and lines from blue to red are values for 2100 under the SSP1-1.9, SSP1-2.6, SSP2-4.5, SSP3-7.0, and SSP5-8.5, respectively. Refer to Figure 2 for the full names of the variable abbreviations on the Y-axes.

remineralization events, or rapid cooling or warming after fast vertical advection) do persist in the surface ocean (Weiss, 1974). For example, sea surface fCO_2 in the Arctic in 2010 was 71–74 µatm (~20%) lower than that in tropical areas (Tables S9 and S10 in Supporting Information S1, Figure 4a; Fransner et al., 2022). This latitudinal difference is projected to gradually decrease. By 2100, the difference between Arctic and tropical surface fCO_2 is projected to be reduced to 19–61 µatm (2%–4%). This is because: (a) the loss of sea ice cover allows more CO_2 to enter the ocean through air-sea gas exchange (Qi et al., 2022; Steinacher et al., 2009; Yamamoto et al., 2012); (b) there is substantial lateral transport of anthropogenic DIC from outside the Arctic (Anderson & Olsen, 2002; Olsen et al., 2015; Terhaar, Orr, Gehlen, et al., 2019; Tjiputra et al., 2010), which could enhance surface ocean fCO_2 in the Arctic and even lead to outgassing of anthropogenic DIC (Caínzos et al., 2022; Terhaar et al., 2020); (c) the loss of sea-ice cover also drives enhanced warming of Arctic waters in summer, which contributes to the rise in summer time seawater fCO_2 through thermodynamics (Carton et al., 2015; Orr et al., 2022; Ouyang et al., 2021); (d) waters outside the Arctic lag the atmospheric CO_2 rise such that there is an increase in the global air-to-sea ΔfCO_2. As in the Arctic Ocean, fCO_2 in the North Atlantic also increases due to cooling of the northward flowing waters and increased anthropogenic DIC in these waters (Caínzos et al., 2022; Völker et al., 2002) (Figure 5).

3.3.2. Total Hydrogen Ion Content ($[H^+]_{total}$)

Seawater acidity is defined by its hydrogen ion content ($[H^+]$), although it is often reported on logarithmic pH scales (Section 3.3.3). However, the logarithmic scale can be misleading when comparing pH changes across domains and timescales, making it necessary to report $[H^+]$ (Fassbender et al., 2021). This model-data fusion product contains both total hydrogen ion content ($[H^+]_{total}$) and free hydrogen ion content ($[H^+]_{free}$). Due to their similar behaviors, only the former is discussed in the text.

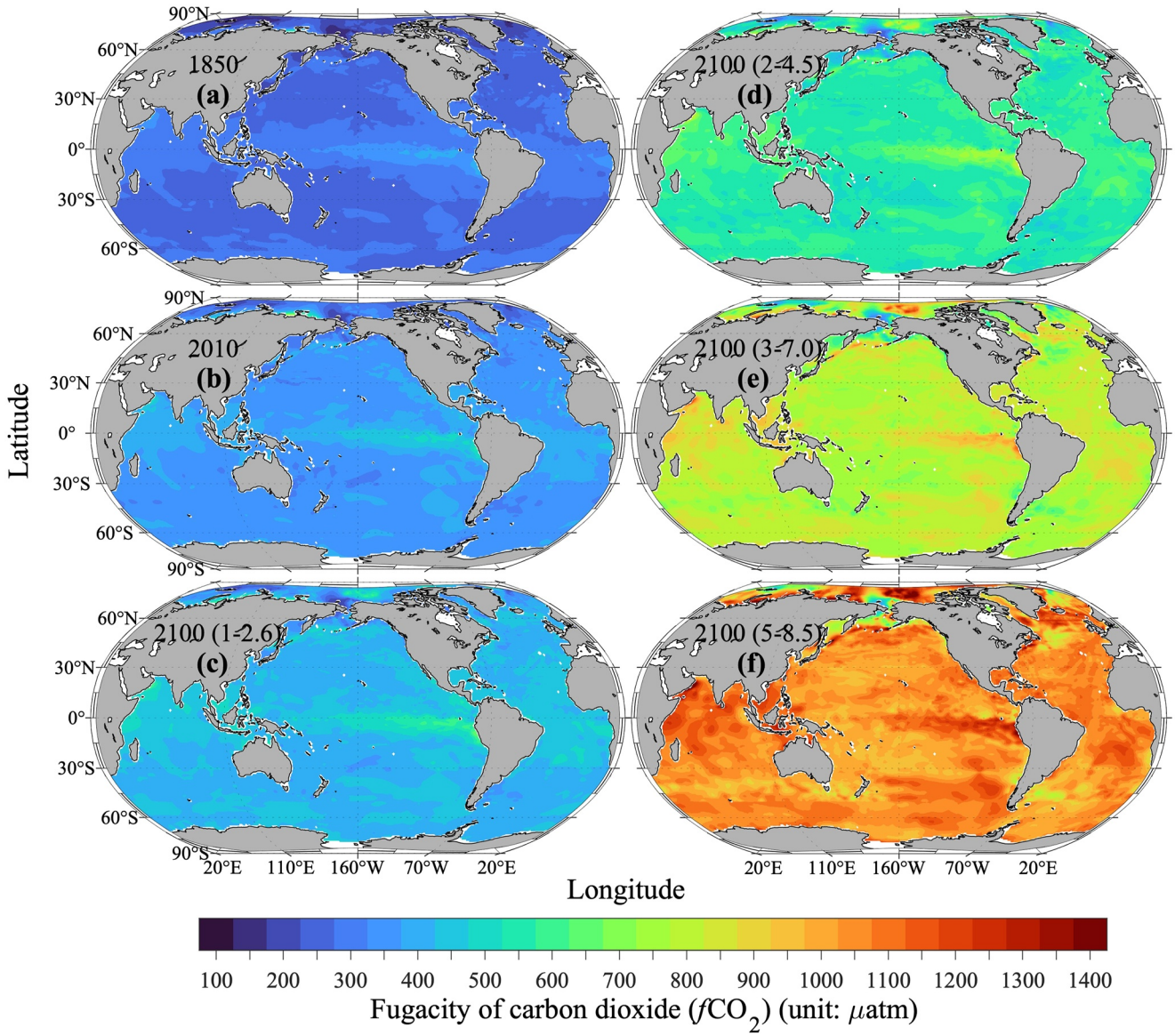

Figure 5. Surface ocean fugacity of carbon dioxide (fCO_2, inter-model median) in the decades around (a) 1850, (b) 2010, (c) 2100 (SSP1-2.6), (d) 2100 (SSP2-4.5), (e) 2100 (SSP3-7.0), and (f) 2100 (SSP5-8.5). SSP is short for Shared Socioeconomic Pathway.

$[H^+]_{total}$ exhibits a nearly perfect linear relationship with fCO_2, within the range of oceanic fCO_2 at current and future conditions (Figure S4 in Supporting Information S1). This linear relationship can be explained by examining the relation between these two quantities from the carbonate system equilibrium equations (Millero, 1995). fCO_2 can be expressed by Equation 2:

$$fCO_2 = \frac{DIC \times [H^+]_{total}}{K_0 K_1 \left(1 + \frac{[H^+]_{total}}{K_1} + \frac{K_2}{[H^+]_{total}}\right)} \quad (2)$$

where K_0 is the solubility coefficient of CO_2 in seawater, and K_1 and K_2 are the first and second dissociation constants of carbonic acid. DIC remains relatively constant, for example, an increase from 2,000 to 2,100 μmol kg^{-1} (e.g., Figure 3c) represents only a change of 5%, and the quantity in parentheses in the denominator ranges from only ~1.05 to ~1.1 for pH_T between ~7.5 and ~8.0. Thus, changes in $[H^+]_{total}$ are driven largely by those in fCO_2 and vice versa, and a nearly linear relationship exists between these two quantities, although the slope of this relationship could vary between waters with different temperatures because of the temperature dependences of K_0 and K_1.

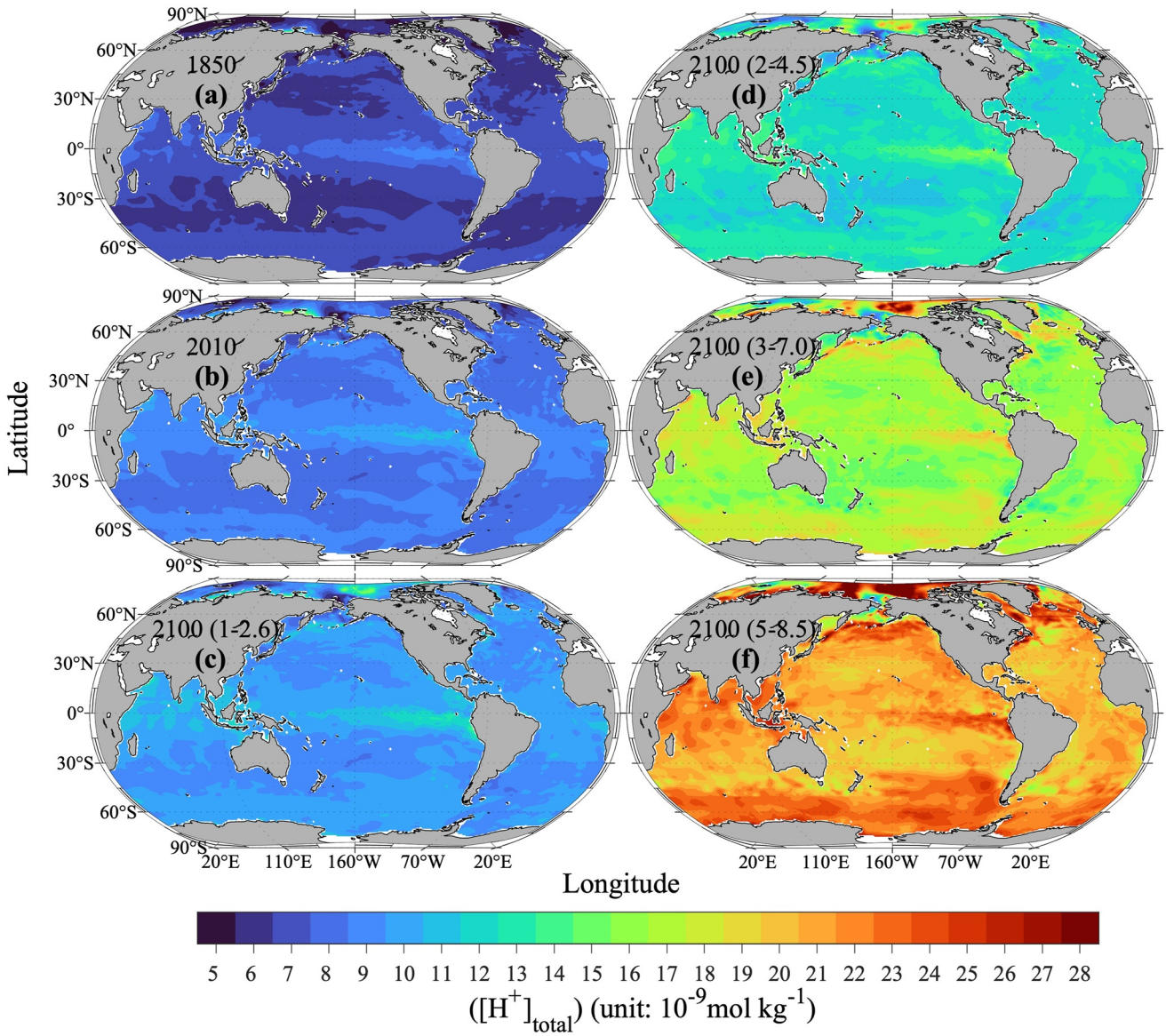

Figure 6. Surface ocean total hydrogen ion content ($[H^+]_{total}$, inter-model median) in the decades around (a) 1850, (b) 2010, (c) 2100 (SSP1-2.6), (d) 2100 (SSP2-4.5), (e) 2100 (SSP3-7.0), and (f) 2100 (SSP5-8.5). SSP is short for Shared Socioeconomic Pathway.

Surface ocean $[H^+]_{total}$ shows relatively homogeneous spatial distributions (Figure 6). From 1750 to 2010 global area-averaged $[H^+]_{total}$ increased by ~30% (from 6.5 to 8.5 × 10^{-9} mol kg^{-1}) (Tables S5—S8 in Supporting Information S1) and will continue to increase by ~4% (to 8.8 × 10^{-9} mol kg^{-1}) under SSP1-1.9 or by ~150% (to 21.2 × 10^{-9} mol kg^{-1}) under SSP5-8.5 (Tables S7, S8, S11, and S12 in Supporting Information S1). The Arctic Ocean shows the fastest increase in $[H^+]_{total}$ (Table S9 and Figure S8 in Supporting Information S1). The area-averaged $[H^+]_{total}$ in the Arctic, which was 15%–20% lower than that in the tropical region during preindustrial period, is projected to become highest among all regions by 2050 under SSP5-8.5 (Tables S9 and S10 in Supporting Information S1). Our results show that acidity in the Arctic will have increased ~50% from 1850 to 2050, compared to ~40% for the rest of the ocean. Because of the nearly linear relation between fCO_2 and $[H^+]_{total}$ (Figure S4 in Supporting Information S1), the relatively large increase of $[H^+]_{total}$ in the Arctic Ocean is similar to that of fCO_2.

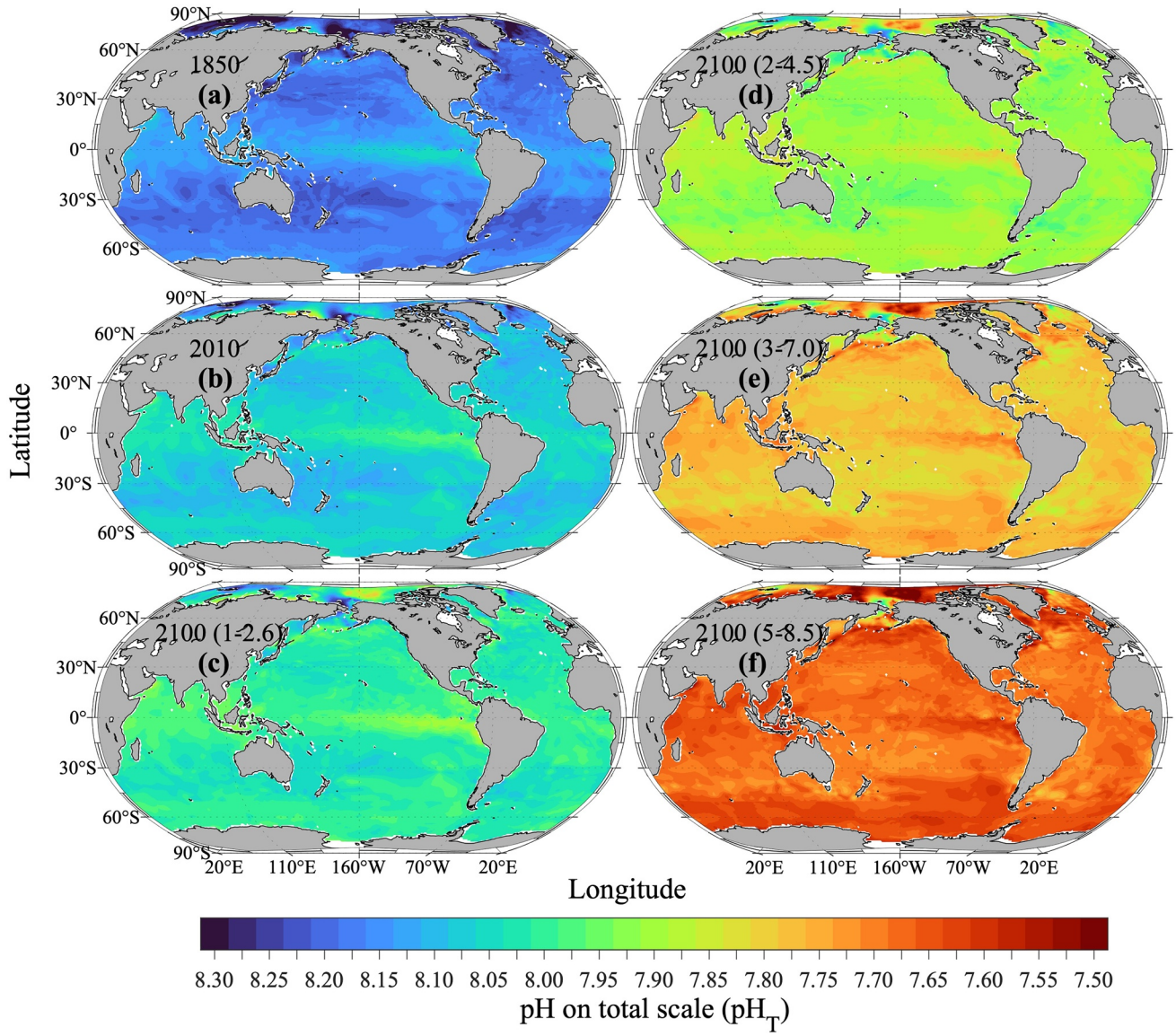

Figure 7. Surface ocean pH on total scale (pH_T, inter-model median) in the decades around (a) 1850, (b) 2010, (c) 2100 (SSP1-2.6), (d) 2100 (SSP2-4.5), (e) 2100 (SSP3-7.0), and (f) 2100 (SSP5-8.5). SSP is short for Shared Socioeconomic Pathway.

3.3.3. pH on Total Scale (pH_T)

Like $[H^+]_{total}$, latitudinal variations of pH_T are relatively small (Figure 7), despite the large temperature gradients from the tropical to the polar regions. This is because although temperature changes affect pH in a closed system (e.g., decreasing temperature elevates pH), this change is compensated by temperature-driven changes in surface ocean DIC that result from air-sea CO_2 fluxes driven by changes in seawater temperature and hence the CO_2 solubility (e.g., colder temperature enables a body of water to absorb more CO_2 in order to maintain equilibrium with the atmosphere, thus increasing its DIC but not TA, affecting the DIC/TA ratio) (Weiss, 1974). These two temperature effects have opposite signs and similar magnitudes, therefore effectively canceling each other (Jiang et al., 2019). Overall, air-sea CO_2 exchange with the globally well-mixed atmosphere tends to dampen regional ocean pH variability, just as it reduces variability in the closely related quantity fCO_2. On the other hand, processes such as upwelling, biological activities, heat exchange, etc., can have a large impact on the local fCO_2 and pH distribution (Feely et al., 2009; Orr et al., 2005), as it takes several months for surface ocean fCO_2 to equilibrate with the atmosphere (Broecker & Peng, 1974).

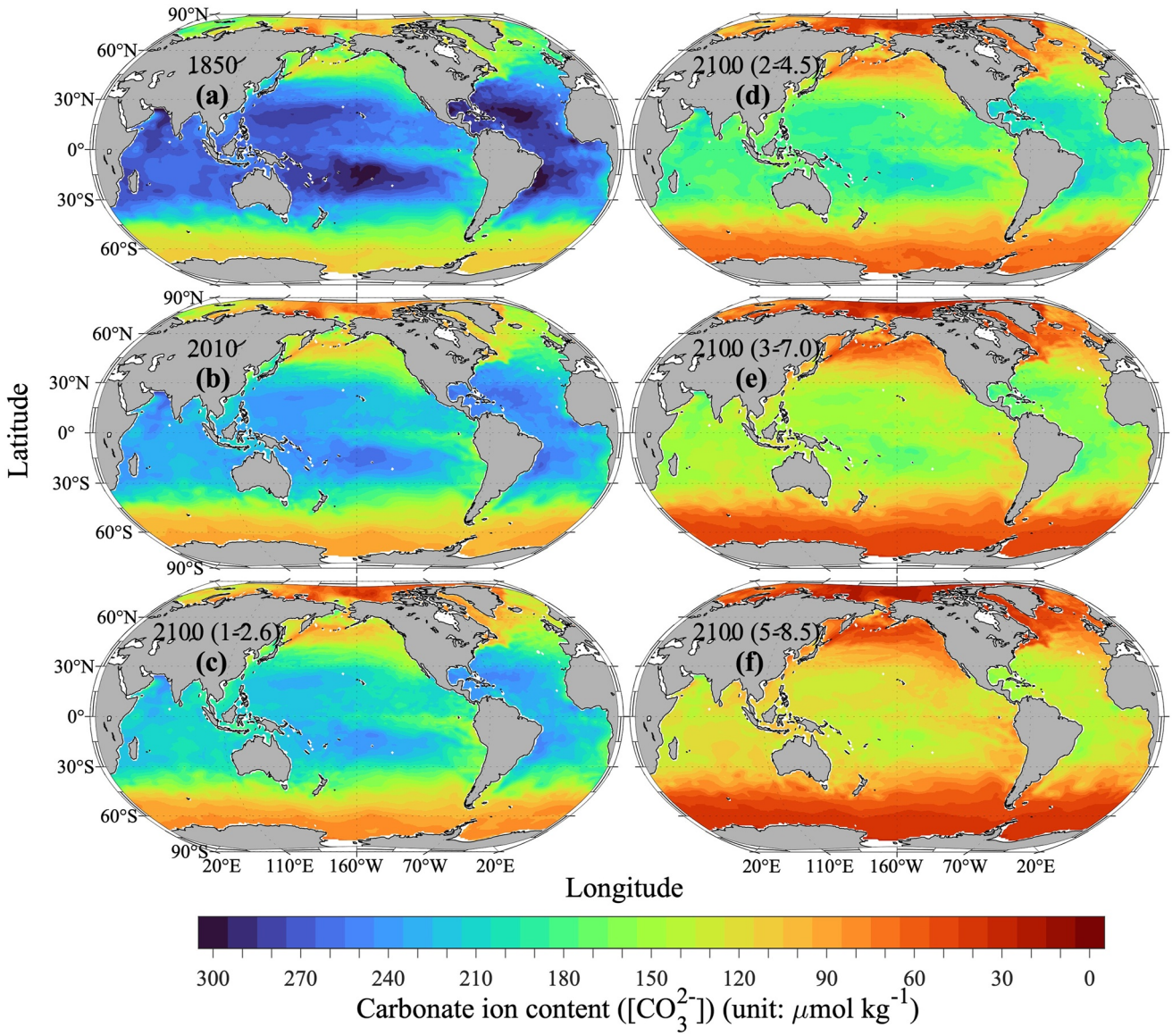

Figure 8. Surface ocean carbonate ion content ($[CO_3^{2-}]$, inter-model median) in the decades around (a) 1850, (b) 2010, (c) 2100 (SSP1-2.6), (d) 2100 (SSP2-4.5), (e) 2100 (SSP3-7.0), and (f) 2100 (SSP5-8.5). SSP is short for Shared Socioeconomic Pathway.

From 1750 to 2010, the area-averaged surface ocean pH_T decreased by ~0.12 units from 8.19 to 8.07 (Tables S5–S8 in Supporting Information S1). The rate of change is slowest in the tropical and subtropical region (−0.11 units) and fastest in the Arctic (−0.14 units) (Figure 4e, Figure S9 in Supporting Information S1). By 2100 the global area-averaged surface ocean pH_T is projected to decrease by 0.01 to 8.06 under SSP1-1.9 or by 0.39 to 7.68 under SSP5-8.5. The latter estimate in 2100 is even lower than the previously reported value of 7.74 under RCP8.5 based on the GFDL-ESM2M model (Jiang et al., 2019). The difference is due to the different land and energy use assumptions that lead to higher atmospheric CO_2 trajectories over the 21st century for the SSPs in CMIP6 than their RCP counterparts in CMIP5 (Meinshausen et al., 2011, 2020) and hence globally and locally greater surface ocean acidification (Kwiatkowski et al., 2020; Terhaar, Torres, et al., 2021).

3.3.4. Carbonate Ion Content ($[CO_3^{2-}]$), and Saturation States of Aragonite (Ω_{arag}) and Calcite (Ω_{calc})

Unlike fCO_2, $[H^+]_{total}$, and pH_T, $[CO_3^{2-}]$ shows a large latitudinal gradient, with values in the tropics being twice as high as those in the Arctic (Figures 4c and 8). Similar to pH_T, $[CO_3^{2-}]$ is strongly controlled by the indirect temperature effect (see Section 3.3.2), that is, colder waters have higher DIC and hence lower $[CO_3^{2-}]$. However,

unlike pH_T, the direct temperature effect leads to a further reduction of $[CO_3^{2-}]$ in colder waters (despite its much smaller magnitude), thus allowing these two effects to reinforce each other (see also Jiang et al., 2019; Orr et al., 2005).

From 1750 to 2010, the global area-averaged $[CO_3^{2-}]$ decreased by ∼16% from 228 to 190 μmol kg^{-1} (Tables S5—S8 in Supporting Information S1). From 2010 to 2100, it is projected to further decrease by 2% to 186 μmol kg^{-1} under SSP1-1.9 or by 48% to 99 μmol kg^{-1} under SSP5-8.5 (Tables S7, and S9–S12 in Supporting Information S1). Regionally, surface ocean $[CO_3^{2-}]$ is projected to decrease more in the tropics (∼100 μmol kg^{-1}) than in the Arctic (∼60 μmol kg^{-1}) from 2010 to 2100 under SSP5-8.5 (Tables S9 and S10 and Figure S10 in Supporting Information S1). The greater decrease in the tropics can largely be attributed to higher initial values there. In fact, the Arctic Ocean shows a stronger relative decrease, that is, ∼60% compared to that of 45%–50% in the tropics (Feely et al., 2009).

$[CO_3^{2-}]$ also mainly determines the saturation states of carbonate minerals (unitless), which are defined as:

$$\Omega = \frac{[Ca^{2+}] \times [CO_3^{2-}]}{K'_{sp}} \quad (3)$$

where Ω is the saturation state (Ω > 1 favors precipitation and Ω < 1 favors dissolution), $[Ca^{2+}]$ is the calcium content, and K'_{sp} is the apparent solubility product of the calcium carbonate mineral. As $[Ca^{2+}]$ in seawater is nearly directly proportional to salinity (Millero, 1995), and K'_{sp} is a function of only temperature and pressure, Ω in surface seawater is nearly directly proportional to $[CO_3^{2-}]$, with a constant of proportionality that depends mostly on temperature.

As a consequence of the nearly linear dependence of Ω_{arag} on $[CO_3^{2-}]$, surface ocean Ω_{arag} shows a similar spatial distribution as $[CO_3^{2-}]$ (Figure S11 in Supporting Information S1). Area-averaged surface ocean Ω_{arag} in 2010 ranges from as high as 3.4–3.6 in tropical regions to as low as 1.5–1.9 in polar regions, similar to previous studies (IPCC, 2013; Jiang et al., 2015; Orr et al., 2005; Steinacher et al., 2009). On average, global surface ocean Ω_{arag} decreased by ∼17% from a global area-average of 3.6 in 1750 to 3.0 in 2010 (Tables S5—S8 in Supporting Information S1). Regionally, the rate of change of Ω_{arag} between 1750 and 2010 ranges from −16% in the tropics to −24% in the Arctic (Table S9 and Figure S12 in Supporting Information S1). From 2010 to 2100, the global area-averaged Ω_{arag} is projected to decrease by 2% to 2.9 under SSP1-1.9 or by 47% to 1.6 under SSP5-8.5 (Tables S7 and S8 in Supporting Information S1). The latter value is lower than the previous estimate of 1.7 under RCP8.5 of the GFDL-ESM2M (Jiang et al., 2019), again due to the higher atmospheric CO_2 under SSP5-8.5 than under RCP8.5. Similar to $[CO_3^{2-}]$, Ω_{arag} shows a larger magnitude of change in the tropics (about −1.6) than in polar regions (about −1.0), although the percentage of change is lower (−44% to −47% compared to −55% to −60%) (Tables S9 and S10 in Supporting Information S1). A comparison of the spatial distribution of the absolute change in this quantity to the percent change is presented in Figure 7 of Feely et al. (2009).

Calcite is a less soluble form of calcium carbonate mineral than aragonite, and at 25°C, Ω_{calc} is ∼50% greater than Ω_{arag} (Mucci, 1983); thus Ω_{calc} shows very similar spatial and temporal variations to Ω_{arag} (Figure S13 in Supporting Information S1). From 1750 to 2010, the global area-averaged Ω_{calc} had also dropped by 17%, and from 2010 to 2100, it is expected to drop further by 2% to 4.5 under SSP1-1.9 or 49% to 2.4 under SSP5-8.5 (Tables S7 and S8 and Figure S14 in Supporting Information S1). Unlike Ω_{arag}, surface Ω_{calc} remained >1 in 2100 under all SSPs except for SSP5-8.5, where undersaturated water ($\Omega_{calc} < 1$) is seen in the Southern Ocean (Figure S13 in Supporting Information S1). However, studies have shown that a rapid change of saturation state and extreme events (Burger et al., 2020, 2022) may affect marine organisms more than the saturation state itself (Doney et al., 2020; Gattuso et al., 2015; Kawahata et al., 2019).

3.3.5. Revelle Factor (RF)

The Revelle Factor (RF), a measure of the ocean's buffer capacity for the carbonate system, is defined as the ratio of the fractional change in fCO_2 to the fractional change in DIC at constant TA (Revelle & Suess, 1957). The higher the RF, the smaller the change in DIC (or mass of carbon taken up by the ocean) for a given change in sea surface fCO_2 (often equilibrated with atmospheric CO_2), reflecting the ocean's lower CO_2 buffering capacity (Broeker et al., 1979).

RF and $[CO_3^{2-}]$ are strongly anti-correlated regionally, because $[CO_3^{2-}]$ buffers the ocean CO_2 uptake (Broekeret al., 1979; Orr et al., 2005). Like $[CO_3^{2-}]$, RF exhibits strong latitudinal gradients, with area-averaged RF in

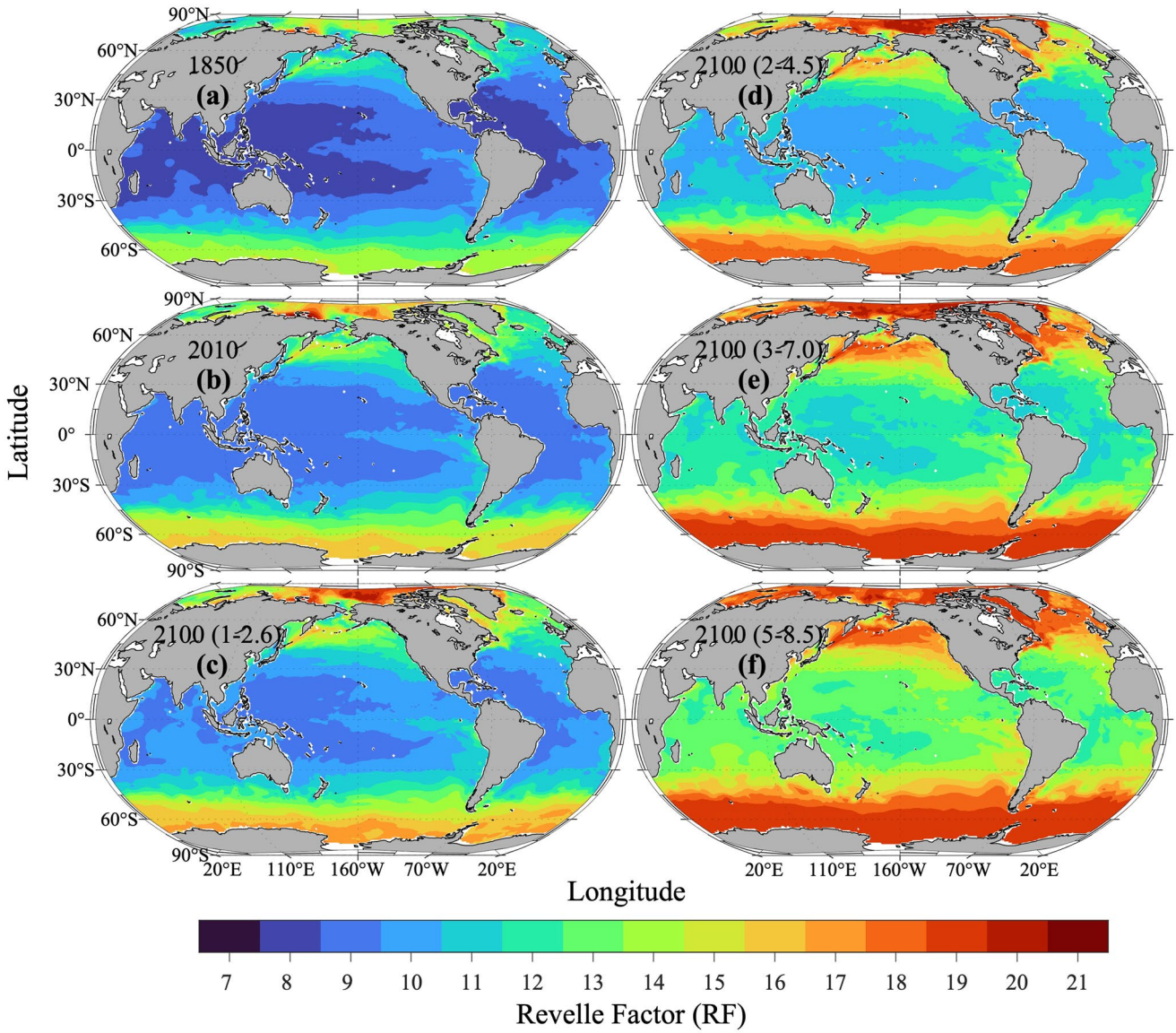

Figure 9. Surface ocean Revelle Factor (RF, inter-model median) in the decades around (a) 1850, (b) 2010, (c) 2100 (SSP1-2.6), (d) 2100 (SSP2-4.5), (e) 2100 (SSP3-7.0), and (f) 2100 (SSP5-8.5). SSP is short for Shared Socioeconomic Pathway.

2010 ranging from ∼9.4 in the tropics (higher buffer capacity) to between 13 and 15 in the polar regions (lower buffer capacity). The latitudinal gradients are projected to strengthen by 2100 under all scenarios (Figure 9). From 1750 to 2010, the global area-averaged RF had increased by 12.5% from 9.6 to 10.8 (Tables S5—S8 in Supporting Information S1). From 2010 to 2100, it is projected to increase by 1% to 10.9 under SSP1-1.9 or by 38% to ∼14.9 under SSP5-8.5 (Tables S7 and S8 and Figure S15 in Supporting Information S1).

3.3.6. Total Dissolved Inorganic Carbon Content (DIC)

As the ocean continues to accumulate anthropogenic CO_2, its DIC—defined as the sum of dissolved carbon dioxide ($[CO_2(aq)]$), bicarbonate ion content ($[HCO_3^-]$), and carbonate ion content ($[CO_3^{2-}]$)—will increase over time. Surface ocean DIC (area-averaged globally) increased by 58 μmol kg^{-1} (3.1%) from the preindustrial level of 1,969 to 2,027 μmol kg^{-1} in 2010 (Tables S5—S8 and Figures S16 and S17 in Supporting Information S1). From 2010 to 2100, surface ocean DIC is projected to increase by 0.2% (5 μmol kg^{-1}) to 2,032 μmol kg^{-1} under SSP1-1.9 or by 7.5% (150 μmol kg^{-1}) to 2177 μmol kg^{-1} under SSP5-8.5 (Tables S7 and S8 in Supporting Information S1).

Regionally, the projected accumulation of DIC over the 21st century (from 2010 to 2100) is lowest in the Arctic (67 μmol kg^{-1}) and Southern oceans (124 μmol kg^{-1}) and strongest in the tropical and subtropical ocean (150–200 μmol kg^{-1}) under SSP5-8.5 (Tables S9 and S10 in Supporting Information S1). The lower accumulation of DIC in the polar regions compared to the tropical and subtropical ocean is due to the higher RF and lower buffer capacity in polar regions because of the relatively higher DIC in colder waters (Figure S16 and Table S9 in Supporting Information S1; Weiss, 1974). The spatial changes in surface ocean DIC also reflect the changes of large scale ocean circulation patterns, for example, the projected slowing of the upper cell of the Atlantic meridional overturning circulations leads to the convergence of surface anthropogenic carbon in the subtropical Atlantic Ocean and less anthropogenic carbon in the subpolar Atlantic Ocean (Tjiputra et al., 2010).

3.3.7. Total Alkalinity Content (TA)

TA is the only OA indicator that is not subject to changes directly associated with air-sea CO_2 exchange. When CO_2 reacts with water, two bicarbonate ions (each with one charge and one equivalent TA unit) are produced for each carbonate ion (two charges, and two equivalent TA units) consumed, thus keeping TA constant:

$$CO_2 + H_2O + CO_3^{2-} \rightleftharpoons 2HCO_3^- \quad (4)$$

Nevertheless, TA plays a pivotal role in ocean buffering, and consequently on the biogeochemical processes governing pH_T, $[H^+]_{total}$, $[H^+]_{free}$, $[CO_3{}^{2-}]$, and saturation states in the ocean (Middelburg et al., 2020).

Across the ESM ensemble, globally area-averaged surface ocean TA does not show a consistent temporal change (Figure S18 in Supporting Information S1 and Figure 2g; Tables S7—S10 in Supporting Information S1). In some models (e.g., GFDL-CM4 and GFDL-ESM4), the removal of alkalinity from the surface ocean through the production of sinking calcium carbonate is assumed to be a positive function of saturation state, that is, the lower the saturation state, the lower the alkalinity removal. Thus, alkalinity content in the surface ocean increases as saturation state decreases. Other models lack saturation dependence (e.g., CESM2), and calcium carbonate production declines in parallel to overall productivity declines, thus increasing alkalinity under climate warming (Kwiatkowski et al., 2020). CMIP6 ESMs with higher TA at present also have higher $[CO_3{}^{2-}]$ and higher buffer capacity (lower RF), and hence show a stronger increase in surface ocean DIC (Terhaar, Frölicher, & Joos, 2022). This larger increase in surface ocean DIC will lead to a stronger decrease of $[CO_3{}^{2-}]$ and a stronger increase of RF over time.

Regionally, however, TA does show consistent temporal changes across the ESM ensemble (Figures S19 and S20 in Supporting Information S1). For example, in the Arctic Ocean, large changes in salinity and TA (driven by melting of sea ice, increased riverine runoff, and enhanced precipitation minus evaporation) are projected by all of the CMIP6 ESMs (Terhaar, Torres, et al., 2021; Wang et al., 2022). Despite the different projections of global ocean TA over the 21st century, these differences remain relatively small compared to changes in DIC due to the increase of atmospheric CO_2 (Figure 1) and hence do not lead to large inter-model differences in the projections of the OA indicators.

3.4. Caveats

Although the latest observational data provide better observational coverage and CMIP6 ESMs simulate more processes explicitly and offer greater spatial resolutions, their use in determining OA indicators comes with important caveats. Observational coverage of biogeochemical variables remains limited and hence leads to uncertainties in the base state in 2010, especially in remote regions such as the Arctic and the Southern Ocean and during winter (Lauvset et al., 2022). Recent developments of statistical methods such as machine learning (e.g., Gregor & Gruber, 2021; Landschützer et al., 2016) might allow extrapolation of biogeochemical measurements in space and time, although such extrapolations also have regional and seasonal biases, especially in undersampled regions (Bushinsky et al., 2019; Gloege et al., 2021; Gregor et al., 2019).

Projections from ESMs also have biases and uncertainties on both regional and global scales. The CMIP6 ESM ensemble includes, for example, a relatively large number of models with high ECS, which likely project an overly strong warming over the 21st century (Tokarska et al., 2020), which may affect projections of temperature-sensitive variables such as $[H^+]$. Biases also exist in the circulation, leading to overly small sea surface salinities and overturning in the Southern Ocean, thus causing biases in OA indicators in that region

(Terhaar, Frölicher, & Joos, 2021). Furthermore, biogeochemical biases across the CMIP6 models exist toward too high surface ocean [CO_3^{2-}] in the equatorial Pacific (Vaittinada Ayar et al., 2022) and too low globally averaged surface ocean [CO_3^{2-}] and TA (Figure 1; Terhaar, Frölicher, & Joos, 2022) and consequently too high globally averaged surface ocean RF (Terhaar, Frölicher, & Joos, 2022). Finally, the reported inter-model median values are not robust in coastal regions (Hauri et al., 2021; Terhaar, Orr, Gehlen, et al., 2019) because of low resolution and non-changing boundary conditions, such as river discharge, and changing DIC, TA, and nutrient fluxes (Terhaar, Orr, Ethé, et al., 2019).

Another inherent caveat of CMIP6 projections is that these projections follow prescribed atmospheric CO_2 mixing ratio trajectories, thus resulting in widely different end-of-century global atmospheric surface temperatures (Tokarska et al., 2020), while global warming policy goals are aiming at limiting global warming to prescribed temperature targets (UNFCCC, 2015). Different simulation set-ups using adaptive emission approaches such as the Adjusting Mitigation Pathway (AMP) (Goodwin et al., 2018) or the Adaptive Emission Reduction Approach (AERA) (Terhaar, Frölicher, Aschwanden, et al., 2022) allow model simulations to converge to a prescribed temperature target. Depending on a model's transient climate response or equilibrium climate sensitivity and the amount of reductions in non-CO_2 greenhouse gas emissions and other radiative agents, the CO_2 emissions and hence CO_2 trajectories that allow reaching a given temperature target vary greatly (Goodwin, 2018; Terhaar, Frölicher, Aschwanden, et al., 2022). These largely different atmospheric CO_2 trajectories lead to uncertainties that exceed the range of model projections under any SSP by an order of magnitude globally (Terhaar et al., 2023) and in the coastal ocean (Nicholls et al., 2018). While such projections with an ESM of Intermediate Complexity Bern3D-LPX (Lienert & Joos, 2018; Roth et al., 2014) and the AERA (Terhaar, Frölicher, Aschwanden, et al., 2022) allow for an estimation for future OA conditions for a given temperature target, regionally more reliable gridded projections of OA for a given policy-relevant warming target could only be achieved by an ensemble of higher-resolved ESMs simulations with the AERA.

Lastly, the product presented here covers only projections of surface OA indicators, although subsurface OA projections are equally important for marine ecosystems, especially for vertically migrating organisms (Berge et al., 2015). Subsurface OA projections across models tend to vary much more than those at the surface because they are often dependent on the ventilation of surface waters to the deeper ocean (Fraser et al., 2022; Steiner et al., 2014; Terhaar et al., 2020, 2021b, 2022a). Subsurface OA projections will be reported in future publications.

4. Conclusions

A model-data fusion product was created by synthesizing 14 CMIP6 ESMs (Table S3 in Supporting Information S1) and three observational data products. This product provides distributions of 10 global surface OA indicators, including fCO_2, pH_T, $[H^+]_{total}$, $[H^+]_{free}$, $[CO_3^{2-}]$, Ω_{arag}, Ω_{calc}, RF, DIC, and TA, under past-reconstruction (1750), historical (1850–2010), and future (2020–2100) scenarios. The model outputs were bias-adjusted with the most recent and highest quality ocean carbon observations available, and drift-adjusted with preindustrial control (piControl) values to highlight the fundamental agreements among the CMIP6 models on the evolution of most carbonate system variables under historical to future scenarios. Despite several caveats, the use of the most recent observational datasets and a large ESM ensemble represents a major step forward in the projection of future surface ocean OA indicators and provides critical information to guide OA mitigation and adaptation efforts.

Data Availability Statement

All model simulations are available at the CMIP6 data portals: https://esgf-node.llnl.gov/projects/cmip6/. Observational data used in this study:

- The Surface Ocean CO_2 Atlas (SOCAT, version 2022): https://www.ncei.noaa.gov/data/oceans/ncei/ocads/metadata/0253659.html (https://doi.org/10.25921/1h9f-nb73).
- The Global Ocean Data Analysis Project version 2 (GLODAPv2, version 2022): https://www.ncei.noaa.gov/data/oceans/ncei/ocads/metadata/0257247.html (https://doi.org/10.25921/1f4w-0t92).
- The Coastal Ocean Data Analysis Product in North America (CODAP-NA, version 2021): https://www.ncei.noaa.gov/data/oceans/ncei/ocads/metadata/0219960.html (https://doi.org/10.25921/531n-c230).
- World Ocean Atlas (2018): https://www.ncei.noaa.gov/access/world-ocean-atlas-2018/.

Acknowledgments
We thank all scientists behind the 14 CMIP6 Earth System Models and those who helped collect and quality control the Surface Ocean CO_2 Atlas (SOCAT, version 2022), the Global Ocean Data Analysis Project Version 2 (GLODAPv2, version 2022), the Coastal Ocean Data Analysis Product in North America (CODAP-NA, version 2021), and the World Ocean Atlas 2018. We acknowledge the World Climate Research Programme, which, through its Working Group on Coupled Modelling, coordinated and promoted CMIP6. We thank the climate modeling groups for producing and making available their model output, the Earth System Grid Federation (ESGF) for archiving the data and providing access, and the multiple funding agencies who support CMIP6 and ESGF. Funding for L-QJ was from NOAA Ocean Acidification Program (OAP, Project ID: 21047) and NOAA National Centers for Environmental Information (NCEI) through a NOAA Cooperative Institute for Satellite Earth System Studies (CISESS) Grant (NA19NES4320002) at the Earth System Science Interdisciplinary Center (ESSIC), University of Maryland. BRC and JDS thank the Global Ocean Monitoring and Observing (GOMO) program (http://data.crossref.org/fundingdata/funder/10.13039/1) of the National Oceanic and Atmospheric Administration for funding their contributions (Project 100007298 and award NA21OAR4310251, respectively) through the Cooperative Institute for Climate, Ocean, and Ecosystem Studies (CIOCES) under NOAA Cooperative Agreement NA20OAR4320271, Contribution 2022-2012. JDS' contributions were partially funded by PMEL, and RAF and SRA's contributions were also funded by GOMO, OAP, and PMEL. Contributions from PMEL are recorded under contribution number 5408. JFT and JS acknowledge the Research Council of Norway (Grants: 270061 and 275268). High-performance storage resources were partly provided by the Norwegian infrastructure for computational science (through projects ns2345k, ns1002k, and ns9560k). JT was funded by the Woods Hole Oceanographic Institution Postdoctoral Scholar Program, the European Union's Horizon 2020 research and innovation program under grant agreement 821003 (project 4C, Climate-Carbon Interactions in the Current Century), and the Swiss National Science Foundation under Grant 200020_200511. AO and SKL appreciate funding from the ICOS-2 project of the Research Council of Norway (project 296012). RS and YS-F thank the support of the team in charge of the CNRM-CM climate model. Supercomputing time was provided by the Meteo-France/DSI supercomputing center. RS acknowledges the European Union's Horizon 2020 research

The generated data product is available in NetCDF format at National Oceanic and Atmospheric Administration (NOAA) National Centers for Environmental Information (NCEI), with a link of https://www.ncei.noaa.gov/data/oceans/ncei/ocads/metadata/0259391.html (https://doi.org/10.25921/9ker-bc48). The data package consists of three folders: (i) "ESMs," which includes bias- and drift-adjusted model output for each of the 14 ESMs; (ii) "median," which contains the inter-model median values of the OA indicators; and (iii) "std," which contains the inter-model standard deviations of the OA indicators. Pre-plotted global maps are also available through this interface: https://www.ncei.noaa.gov/access/ocean-carbon-acidification-data-system/synthesis/surface-oa-indicators.html.

References

Albright, R., Caldeira, L., Hosfelt, J., Kwiatkowski, L., Maclaren, J. K., Mason, B. M., et al. (2016). Reversal of ocean acidification enhances net coral reef calcification. *Nature*, *531*(7594), 362–365. https://doi.org/10.1038/nature17155

Anderson, L. G., & Olsen, A. (2002). Air-sea flux of anthropogenic carbon dioxide in the North Atlantic. *Geophysical Research Letters*, *29*(17), 16-1–16-4. https://doi.org/10.1029/2002gl014820

Andersson, A. J., & Gledhill, D. (2013). Ocean acidification and coral reefs: Effects on breakdown, dissolution, and Net Ecosystem Calcification. *Annual Review of Marine Science*, *5*(1), 321–348. https://doi.org/10.1146/annurev-marine-121211-172241

Bakker, D. C. E., Pfeil, B., Landa, C. S., Metzl, N., O'Brien, K. M., Olsen, A., et al. (2016). A multi-decade record of high-quality fCO_2 data in version 3 of the Surface Ocean CO_2 Atlas (SOCAT). *Earth System Science Data*, *8*(2), 383–413. https://doi.org/10.5194/essd-8-383-2016

Barth, A., Beckers, J.-M., Troupin, C., Alvera-Azcárate, A., & Vandenbulcke, L. (2014). DIVAnd-1.0: N-dimensional variational data analysis for ocean observations. *Geoscientific Model Development*, *7*(1), 225–241. https://doi.org/10.5194/gmd-7-225-2014

Berge, J., Renaud, P. E., Darnis, G., Cottier, F., Last, K., Gabrielsen, T. M., et al. (2015). In the dark: A review of ecosystem processes during the Arctic polar night. *Progress in Oceanography*, *139*, 258–271. https://doi.org/10.1016/j.pocean.2015.08.005

Broecker, W. S., & Peng, T.-H. (1974). Gas exchange rates between air and sea. *Tellus*, *26*(1–2), 21–35. https://doi.org/10.1111/j.2153-3490.1974.tb01948.x

Broecker, W. S., Takahashi, T., Simpson, H. J., & Peng, T.-H. (1979). Fate of fossil fuel carbon dioxide and the Global Carbon Budget. *Science*, *206*(4417), 409–418. https://doi.org/10.1126/science.206.4417.409

Burger, F. A., John, J. G., & Frölicher, T. L. (2020). Increase in ocean acidity variability and extremes under increasing atmospheric CO_2. *Biogeosciences*, *17*(18), 4633–4662. https://doi.org/10.5194/bg-17-4633-2020

Burger, F. A., Terhaar, J., & Frölicher, T. L. (2022). Compound marine heatwaves and ocean acidity extremes. *Nature Communications*, *13*(1), 4722. https://doi.org/10.1038/s41467-022-32120-7

Bushinsky, S. M., Landschützer, P., Rödenbeck, C., Gray, A. R., Baker, D., Mazloff, M. R., et al. (2019). Reassessing southern ocean air-sea CO_2 flux estimates with the addition of Biogeochemical Float Observations. *Global Biogeochemical Cycles*, *33*(11), 1370–1388. https://doi.org/10.1029/2019gb006176

Caínzos, V., Velo, A., Pérez, F. F., & Hernández-Guerra, A. (2022). Anthropogenic carbon transport variability in the Atlantic Ocean over three decades. *Global Biogeochemical Cycles*, *36*(11). https://doi.org/10.1029/2022gb007475

Caldeira, K., & Berner, R. (1999). Seawater pH and atmospheric carbon dioxide. *Science*, *286*(5447), 2043. https://doi.org/10.1126/science.286.5447.2043a

Caldeira, K., & Wickett, M. E. (2003). Anthropogenic carbon and ocean pH. *Nature*, *425*(6956), 365. https://doi.org/10.1038/425365a

Carter, B. R., Bittig, H. C., Fassbender, A. J., Sharp, J. D., Takeshita, Y., Xu, Y.-Y., et al. (2021). New and updated global empirical seawater property estimation routines. *Limnology and Oceanography: Methods*, *19*(12), 785–809. https://doi.org/10.1002/lom3.10461

Carter, B. R., Williams, N. L., Gray, A. R., & Feely, R. A. (2016). Locally interpolated alkalinity regression for global alkalinity estimation. *Limnology and Oceanography: Methods*, *14*(4), 268–277. https://doi.org/10.1002/lom3.10087

Carton, J. A., Ding, Y., & Arrigo, K. R. (2015). The seasonal cycle of the Arctic Ocean under climate change. *Geophysical Research Letters*, *42*(18), 7681–7686. https://doi.org/10.1002/2015gl064514

Connell, S. D., Doubleday, Z. A., Foster, N. R., Hamlyn, S. B., Harley, C. D., Helmuth, B., et al. (2018). The duality of ocean acidification as a resource and a stressor. *Ecology*, *99*(5), 1005–1010. https://doi.org/10.1002/ecy.2209

DeVries, T. (2022). The ocean carbon cycle. *Annual Review of Environment and Resources*, *47*(1), 317–341. https://doi.org/10.1146/annurev-environ-120920-111307

Dickson, A. G. (1990). Standard potential of the reaction: $AgCl(s) + 1/2\ H_2(g) = Ag(s) + HCl(aq)$, and the standard acidity constant of the ion HSO_4^- in synthetic seawater from 273.15 to 318.15K. *Journal of Chemical Thermodynamics*, *22*(2), 113–127. https://doi.org/10.1016/0021-9614(90)90074-Z

Doney, S. C., Busch, D. S., Cooley, S. R., & Kroeker, K. J. (2020). The impacts of ocean acidification on marine ecosystems and reliant human communities. *Annual Review of Environment and Resources*, *45*(1), 83–112. https://doi.org/10.1146/annurev-environ-012320-083019

Doney, S. C., Fabry, V. J., Feely, R. A., & Kleypas, J. A. (2009). Ocean acidification: The other CO_2 problem. *Annual Review of Marine Science*, *1*, 169–192. https://doi.org/10.1146/annurev.marine.010908.163834

Drake, T. W., Tank, S. E., Zhulidov, A. V., Holmes, R. M., Gurtovaya, T., & Spencer, R. G. (2018). Increasing alkalinity export from large Russian Arctic Rivers. *Environmental Science and Technology*, *52*(15), 8302–8308. https://doi.org/10.1021/acs.est.8b01051

Dunne, J. P., Bociu, I., Bronselaer, B., Guo, H., John, J. G., Krasting, J. P., et al. (2020). Simple global ocean biogeochemistry with light, iron, nutrients and gas version 2 (blingv2): Model description and simulation characteristics in GFDL's CM4.0. *Journal of Advances in Modeling Earth Systems*, *12*(10). https://doi.org/10.1029/2019ms002008

Dunne, J. P., Horowitz, L. W., Adcroft, A. J., Ginoux, P., Held, I. M., John, J. G., et al. (2020). The GFDL Earth System Model Version 4.1 (GFDL-ESM 4.1): Overall coupled model description and simulation characteristics. *Journal of Advances in Modeling Earth Systems*, *12*(11). https://doi.org/10.1029/2019MS002015

Dunne, J. P., John, J. G., Shevliakova, E., Stouffer, R. J., Krasting, J. P., Malyshev, S. L., et al. (2013). GFDL's ESM2 global coupled climate–carbon Earth system models. Part II: Carbon system formulation and baseline simulation characteristics. *Journal of Climate*, *26*(7), 2247–2267. https://doi.org/10.1175/jcli-d-12-00150.1

Durack, P. J., Wijffels, S. E., & Matear, R. J. (2012). Ocean salinities reveal strong global water cycle intensification during 1950 to 2000. *Science*, *336*(6080), 455–458. https://doi.org/10.1126/science.1212222

and innovation program under grant agreement 101003536 (ESM2025—Earth System Models for the Future). YS-F acknowledges the TRIATLAS project under the grant agreement 817578 and the COMFORT project under the grant agreement 820989. MW and AY acknowledge the Integrated Research Program for Advancing Climate Models (TOUGOU) Grant JPMXD0717935715 from the Ministry of Education, Culture, Sports, Science and Technology (MEXT), Japan. TZ received funding from the Australian Government under the National Environmental Science Program. Alex Kozyr, who is partially funded by NOAA Global Ocean Monitoring and Observing Program (GOMO), provided data management support for all three aforementioned observational data products, as well as the newly developed data product. We thank Huan Guo (NOAA Geophysical Fluid Dynamic Laboratory, Princeton, New Jersey, United States) for answering questions about the GFDL-CM4 Model; Olivier Boucher of Center Institut Pierre-Simon Laplace (Guyancourt, France) for answering questions about the IPSL-CM6A-LR Model, and Alistair Sellar of Met Office Hadley Centre for Climate Science and Services (Exeter, Devon, United Kingdom) for answering questions about the piControl data of the UKESM1 Model. We thank Dr. Dwight Gledhill and Liza Wright-Fairbank for offering comments on the web interface to display the plotted maps.

Etheridge, D. M., Steele, L. P., Langenfelds, R. L., Francey, R. J., Barnola, J.-M., & Morgan, V. I. (1996). Natural and anthropogenic changes in atmospheric CO_2 over the last 1000 years from air in Antarctic Ice and firn. *Journal of Geophysical Research*, *101*(D2), 4115–4128. https://doi.org/10.1029/95jd03410

Eyring, V., Bony, S., Meehl, G. A., Senior, C. A., Stevens, B., Stouffer, R. J., & Taylor, K. E. (2016). Overview of the coupled model intercomparison project phase 6 (CMIP6) experimental design and organization. *Geoscientific Model Development*, *9*(5), 1937–1958. https://doi.org/10.5194/gmd-9-1937-2016

Fabry, V., McClintock, J., Mathis, J., & Grebmeier, J. (2009). Ocean acidification at high latitudes: The Bellwether. *Oceanography*, *22*(4), 160–171. https://doi.org/10.5670/oceanog.2009.105

Fassbender, A. J., Orr, J. C., & Dickson, A. G. (2021). Technical note: Interpreting pH changes. *Biogeosciences*, *18*(4), 1407–1415. https://doi.org/10.5194/bg-18-1407-2021

Feely, R., Doney, S., & Cooley, S. (2009). Ocean acidification: Present conditions and future changes in a high-CO_2 world. *Oceanography*, *22*(4), 36–47. https://doi.org/10.5670/oceanog.2009.95

Feely, R. A., Jiang, L.-Q., Wanninkhof, R., Carter, B. R., Alin, S., Bednaršek, N., & Cosca, C. E. (2023). Acidification of the global surface ocean: What we have learned from observations. *Oceanography*. in prep.

Feely, R. A., Sabine, C. L., Lee, K., Berelson, W., Kleypas, J., Fabry, V. J., & Millero, F. J. (2004). Impact of anthropogenic CO_2 on the $CaCO_3$ system in the oceans. *Science*, *305*(5682), 362–366. https://doi.org/10.1126/science.1097329

Fransner, F., Fröb, F., Tjiputra, J., Goris, N., Lauvset, S. K., Skjelvan, I., et al. (2022). Acidification of the Nordic Seas. *Biogeosciences*, *19*(3), 979–1012. https://doi.org/10.5194/bg-19-979-2022

Fraser, N. J., Cunningham, S. A., Drysdale, L. A., Inall, M. E., Johnson, C., Jones, S. C., et al. (2022). North Atlantic Current and European slope current circulation in the Rockall Trough observed using moorings and gliders. *Journal of Geophysical Research: Oceans*, *127*(12). https://doi.org/10.1029/2022jc019291

Friedlingstein, P., O'Sullivan, M., Jones, M. W., Andrew, R. M., Gregor, L., Hauck, J., et al. (2022). Global carbon budget 2021. *Earth System Science Data*, *14*(11), 4811–4900. https://doi.org/10.5194/essd-14-4811-2022

Garcia, H. E., Boyer, T. P., Baranova, O. K., Locarnini, R. A., Mishonov, A. V., Grodsky, A., et al. (2019). In A. Mishonov (Ed.), *World Ocean Atlas 2018: Product documentation* (p. 20). Silver Spring. Retrieved from https://www.ncei.noaa.gov/data/oceans/woa/WOA18/DOC/woa18documentation.pdf

Gattuso, J.-P., & Hansson, L. (2011). *Ocean acidification* (p. 326). Oxford University Press.

Gattuso, J.-P., Magnan, A., Billé, R., Cheung, W. W., Howes, E. L., Joos, F., et al. (2015). Contrasting futures for ocean and society from different anthropogenic CO_2 emissions scenarios. *Science*, *349*(6243), aac4722. https://doi.org/10.1126/science.aac472

Gloege, L., McKinley, G. A., Landschützer, P., Fay, A. R., Frölicher, T. L., Fyfe, J. C., et al. (2021). Quantifying errors in observationally based estimates of Ocean Carbon Sink variability. *Global Biogeochemical Cycles*, *35*(4). https://doi.org/10.1029/2020gb006788

Goodwin, P. (2018). On the time evolution of climate sensitivity and future warming. *Earth's Future*, *6*(9), 1336–1348. https://doi.org/10.1029/2018ef000889

Goodwin, P., Brown, S., Haigh, I. D., Nicholls, R. J., & Matter, J. M. (2018). Adjusting mitigation pathways to stabilize climate at 1.5°C and 2.0°C rise in global temperatures to year 2300. *Earth's Future*, *6*(3), 601–615. https://doi.org/10.1002/2017ef000732

Gregor, L., & Gruber, N. (2021). Oceansoda-ETHZ: A global gridded data set of the surface ocean carbonate system for seasonal to decadal studies of Ocean Acidification. *Earth System Science Data*, *13*(2), 777–808. https://doi.org/10.5194/essd-13-777-2021

Gregor, L., Lebehot, A. D., Kok, S., & Scheel Monteiro, P. M. (2019). A comparative assessment of the uncertainties of Global Surface Ocean CO_2 estimates using a machine-learning ensemble (CSIR-ML6 version 2019a) – Have we hit the wall? *Geoscientific Model Development*, *12*(12), 5113–5136. https://doi.org/10.5194/gmd-12-5113-2019

Gruber, N., Bakker, D. C., DeVries, T., Gregor, L., Hauck, J., Landschützer, P., et al. (2023). Trends and variability in the ocean carbon sink. *Nature Reviews Earth & Environment*, *4*(2), 119–134. https://doi.org/10.1038/s43017-022-00381-x

Gruber, N., Clement, D., Carter, B. R., Feely, R. A., van Heuven, S., Hoppema, M., et al. (2019). The oceanic sink for anthropogenic CO_2 from 1994 to 2007. *Science*, *363*(6432), 1193–1199. https://doi.org/10.1126/science.aau5153

Hassell, D., Gregory, J., Blower, J., Lawrence, B. N., & Taylor, K. E. (2017). A data model of the climate and forecast metadata conventions (CF-1.6) with a software implementation (CF-python v2.1). *Geoscientific Model Development*, *10*(12), 4619–4646. https://doi.org/10.5194/gmd-10-4619-2017

Hauri, C., Pagès, R., McDonnell, A. M., Stuecker, M. F., Danielson, S. L., Hedstrom, K., et al. (2021). Modulation of ocean acidification by decadal climate variability in the Gulf of Alaska. *Communications Earth and Environment*, *2*(1), 191. https://doi.org/10.1038/s43247-021-00254-z

Held, I. M., Guo, H., Adcroft, A., Dunne, J. P., Horowitz, L. W., Krasting, J., et al. (2019). Structure and performance of GFDL's CM4. 0 climate model. *Journal of Advances in Modeling Earth Systems*, *11*(11), 3691–3727. https://doi.org/10.1029/2019MS001829

Humphreys, M. P., Orr, J. C., van Heuven, S. M. A. C., Pierrot, D., Lewis, E. R., & Wallace, D. W. R. (2022). *mvdh7/CO2System.jl: CO2System.jl: CO2SYS in Julia (v2.0.5-jl.1)*. Zenodo. https://doi.org/10.5281/zenodo.6395674

Ilyina, T., Zeebe, R. E., Maier-Reimer, E., & Heinze, C. (2009). Early detection of ocean acidification effects on marine calcification. *Global Biogeochemical Cycles*, *23*(1). https://doi.org/10.1029/2008gb003278

IOC, SCOR, & IAPSO. (2010). The International Thermodynamic Equation of Seawater - 2010: Calculation and use of thermodynamic properties. *Intergovernmental Oceanographic Commission, Manuals and guides No. 56*. UNESCO.196.

IPCC. (2000). *Intergovernmental panel on climate change (IPCC) IS92 emissions scenarios (A, B, C, D, E, F) dataset version 1.1. Palisades*. NASA Socioeconomic Data and Applications Center (SEDAC). https://doi.org/10.7927/H41C1TT4

IPCC. (2013). In T. F. Stocker, D. Qin, G.-K. Plattner, M. Tignor, S. K. Allen, et al. (Eds.), *Climate Change 2013: The Physical Science Basis. Contribution of Working Group I to the Fifth Assessment Report of the Intergovernmental Panel on Climate Change*. Cambridge University Press.1535.

IPCC. (2021). In V. Masson-Delmotte, P. Zhai, A. Pirani, S. L. Connors, C. Péan, et al. (Eds.), *Climate Change 2021: The Physical Science Basis. Contribution of Working Group I to the Sixth Assessment Report of the Intergovernmental Panel on Climate Change*. Cambridge University Press.

IPCC. (2022). In H.-O. Pörtner, D. C. Roberts, M. Tignor, E. S. Poloczanska, K. Mintenbeck, et al. (Eds.), *Climate Change 2022: Impacts, Adaptation, and Vulnerability. Contribution of Working Group II to the Sixth Assessment Report of the Intergovernmental Panel on Climate Change*. Cambridge University Press.

Jiang, L.-Q., Carter, B. R., Feely, R. A., Lauvset, S., & Olsen, A. (2019). Surface ocean pH and buffer capacity: Past, present and future. *Scientific Reports*, *9*(1), 18624. https://doi.org/10.1038/s41598-019-55039-4

Jiang, L.-Q., Feely, R. A., Carter, B. R., Greeley, D. J., Gledhill, D. K., & Arzayus, K. M. (2015). Climatological distribution of aragonite saturation state in the global oceans. *Global Biogeochemical Cycles*, *29*(10), 1656–1673. https://doi.org/10.1002/2015GB005198

Jiang, L.-Q., Feely, R. A., Wanninkhof, R., Greeley, D., Barbero, L., Alin, S., et al. (2021). Coastal ocean data analysis product in North America (CODAP-NA) – An internally consistent data product for discrete inorganic carbon, oxygen, and nutrients on the North American ocean margins. *Earth System Science Data*, *13*(6), 2777–2799. https://doi.org/10.5194/essd-13-2777-2021

Jiang, L.-Q., Pierrot, D., Wanninkhof, R., Feely, R. A., Tilbrook, B., Alin, S., et al. (2022). Best practice data standards for discrete chemical oceanographic observations. *Frontiers in Marine Science*, *8*, 705638. https://doi.org/10.3389/fmars.2021.705638

Kawahata, H., Fujita, K., Iguchi, A., Inoue, M., Iwasaki, S., Kuroyanagi, A., et al. (2019). Perspective on the response of marine calcifiers to global warming and ocean acidification—Behavior of corals and foraminifera in a high CO_2 world "hot house". *Progress in Earth and Planetary Science*, *6*(1), 5. https://doi.org/10.1186/s40645-018-0239-9

Kroeker, K., Kordas, R., Crim, R., Hendriks, I., Ramajo, L., Singh, G., et al. (2013). Impacts of ocean acidification on marine organisms: Quantifying sensitivities and interaction with warming. *Global Change Biology*, *19*(6), 1884–1896. https://doi.org/10.1111/gcb.12179

Kwiatkowski, L., Torres, O., Bopp, L., Aumont, O., Chamberlain, M., Christian, J. R., et al. (2020). Twenty-first century ocean warming, acidification, deoxygenation, and upper-ocean nutrient and primary production decline from CMIP6 model projections. *Biogeosciences*, *17*(13), 3439–3470. https://doi.org/10.5194/bg-17-3439-2020

Landschützer, P., Gruber, N., & Bakker, D. C. E. (2016). Decadal variations and trends of the global ocean carbon sink. *Global Biogeochemical Cycles*, *30*(10), 1396–1417. https://doi.org/10.1002/2015GB005359

Lauvset, S. K., Lange, N., Tanhua, T., Bittig, H. C., Olsen, A., Kozyr, A., et al. (2022). GLODAPv2.2022: The latest version of the global interior ocean biogeochemical data product. *Earth System Science Data*, *14*(12), 5543–5572. https://doi.org/10.5194/essd-14-5543-2022

Lee, K., Kim, T.-W., Byrne, R. H., Millero, F. J., Feely, R. A., & Liu, Y.-M. (2010). The universal ratio of boron to chlorinity for the North Pacific and North Atlantic oceans. *Geochimica et Cosmochimica Acta*, *74*(6), 1801–1811. https://doi.org/10.1016/j.gca.2009.12.027

Lienert, S., & Joos, F. (2018). A Bayesian ensemble data assimilation to constrain model parameters and land-use carbon emissions. *Biogeosciences*, *15*(9), 2909–2930. https://doi.org/10.5194/bg-15-2909-2018

Lueker, T. J., Dickson, A. G., & Keeling, C. D. (2000). Ocean pCO_2 calculated from dissolved inorganic carbon, alkalinity, and equations for K_1 and K_2: Validation based on laboratory measurements of CO_2 in gas and seawater at equilibrium. *Marine Chemistry*, *70*(1–3), 105–119. https://doi.org/10.1016/s0304-4203(00)00022-0

MacFarling Meure, C., Etheridge, D., Trudinger, C., Steele, P., Langenfelds, R., van Ommen, T., et al. (2006). Law dome CO_2, CH_4 and N_2O ice core records extended to 2000 years BP. *Geophysical Research Letters*, *33*(14), L14810. https://doi.org/10.1029/2006gl026152

McDougall, T. J., & Barker, P. M. (2011). Getting started with TEOS-10 and the Gibbs seawater (GSW) oceanographic toolbox. SCOR/IAPSO WG127. 28 Retrieved from https://www.teos-10.org/pubs/Getting_Started.pdf. accessed November 2021.

Meinshausen, M., Nicholls, Z. R. J., Lewis, J., Gidden, M. J., Vogel, E., Freund, M., et al. (2020). The shared socioeconomic pathway (SSP) greenhouse gas concentrations and their extensions to 2500. *Geoscientific Model Development*, *13*(8), 3571–3605. https://doi.org/10.5194/gmd-13-3571-2020

Meinshausen, M., Smith, S. J., Calvin, K., Daniel, J. S., Kainuma, M., Lamarque, J.-F., et al. (2011). The RCP greenhouse gas concentrations and their extensions from 1765 to 2300. *Climate Change*, *109*(1–2), 213–241. https://doi.org/10.1007/s10584-011-0156-z

Middelburg, J. J., Soetaert, K., & Hagens, M. (2020). Ocean alkalinity, buffering and biogeochemistry. *Reviews of Geophysics*, *58*(3), e2019RG000681. https://doi.org/10.1029/2019RG000681

Millero, F. J. (1995). Thermodynamics of the carbon dioxide system in the oceans. *Geochimica et Cosmochimica Acta*, *59*(4), 661–677. https://doi.org/10.1016/0016-7037(94)00354-o

Mucci, A. (1983). The solubility of calcite and aragonite in seawater at various salinities, temperature, and one atmosphere total pressure. *American Journal of Science*, *238*, 780–799. https://doi.org/10.2475/ajs.283.7.780

Nicholls, R. J., Brown, S., Goodwin, P., Wahl, T., Lowe, J., Solan, M., et al. (2018). Stabilization of global temperature at 1.5°C and 2.0°C: Implications for coastal areas. *Philosophical Transactions of the Royal Society A: Mathematical, Physical & Engineering Sciences*, *376*(2119), 20160448. https://doi.org/10.1098/rsta.2016.0448

Nijsse, F. J., Cox, P. M., & Williamson, M. S. (2020). Emergent constraints on transient climate response (TCR) and Equilibrium Climate sensitivity (ECS) from historical warming in CMIP5 and CMIP6 models. *Earth System Dynamics*, *11*(3), 737–750. https://doi.org/10.5194/esd-11-737-2020

Olsen, A., Anderson, L. G., & Heinze, C. (2015). Arctic carbon cycle: Patterns, impacts and possible changes. *The New Arctic*, *95*, 115. https://doi.org/10.1007/978-3-319-17602-4_8

O'Neill, B. C., Kriegler, E., Riahi, K., Ebi, K. L., Hallegatte, S., Carter, T. R., et al. (2014). A new scenario framework for climate change research: The concept of shared socioeconomic pathways. *Climatic Change*, *122*(3), 387–400. https://doi.org/10.1007/s10584-013-0905-2

O'Neill, B. C., Tebaldi, C., van Vuuren, D. P., Eyring, V., Friedlingstein, P., Hurtt, G., et al. (2016). The Scenario Model Intercomparison Project (ScenarioMIP) for CMIP6. *Geoscientific Model Development*, *9*, 3461–3482. https://doi.org/10.5194/gmd-9-3461-2016

Orr, J. C., Epitalon, J.-M., Dickson, A. G., & Gattuso, J.-P. (2018). Routine uncertainty propagation for the marine carbon dioxide system. *Marine Chemistry*, *207*, 84–107. https://doi.org/10.1016/j.marchem.2018.10.006

Orr, J. C., Fabry, V. J., Aumont, O., Bopp, L., Doney, S. C., Feely, R. A., et al. (2005). Anthropogenic ocean acidification over the twenty-first century and its impact on calcifying organisms. *Nature*, *437*(7059), 681–686. https://doi.org/10.1038/nature04095

Orr, J. C., Kwiatkowski, L., & Pörtner, H.-O. (2022). Arctic Ocean annual high in pCO2 could shift from winter to summer. *Nature*, *610*(7930), 94–100. https://doi.org/10.1038/s41586-022-05205-y

Ouyang, Z., Qi, D., Zhong, W., Chen, L., Gao, Z., Lin, H., et al. (2021). Summertime evolution of net community production and CO_2 flux in the Western Arctic Ocean. *Global Biogeochemical Cycles*, *35*(3). https://doi.org/10.1029/2020gb006651

Perez, F. F., & Fraga, F. (1987). Association constant of fluoride and hydrogen ions in seawater. *Marine Chemistry*, *21*(2), 161–168. https://doi.org/10.1016/0304-4203(87)90036-3

Planchat, A., Kwiatkwoski, L., Bopp, L., Torres, O., Christian, J. R., Butenschön, M., et al. (2022). The representation of alkalinity and the carbonate pump from CMIP5 to CMIP6 ESMs and implications for the ocean carbon cycle. *EGUsphere*, 1–76. https://doi.org/10.5194/egusphere-2022-1041

Qi, D., Ouyang, Z., Chen, L., Wu, Y., Lei, R., Chen, B., et al. (2022). Climate change drives rapid decadal acidification in the Arctic Ocean from 1994 to 2020. *Science*, *377*(6614), 1544–1550. https://doi.org/10.1126/science.abo0383

Revelle, R., & Suess, H. E. (1957). Carbon dioxide exchange between atmosphere and ocean and the question of an increase of atmospheric CO_2 during the past decades. *Tellus*, *9*(1), 18–27. https://doi.org/10.3402/tellusa.v9i1.9075

Riahi, K., Rao, S., Krey, V., Cho, C., Chirkov, V., Fischer, G., et al. (2011). RCP 8.5—A scenario of comparatively high greenhouse gas emissions. *Climatic Change*, *109*(1–2), 33–57. https://doi.org/10.1007/s10584-011-0149-y

Riahi, K., van Vuuren, D. P., Kriegler, E., Edmonds, J., O'Neill, B. C., Fujimori, S., et al. (2017). The Shared Socioeconomic Pathways and their energy, land use, and greenhouse gas emissions implications: An overview. *Global Environmental Change*, *42*, 153–168. https://doi.org/10.1016/j.gloenvcha.2016.05.009

Roth, R., Ritz, S. P., & Joos, F. (2014). Burial-nutrient feedbacks amplify the sensitivity of atmospheric carbon dioxide to changes in organic matter remineralisation. *Earth System Dynamics*, *5*(2), 321–343. https://doi.org/10.5194/esd-5-321-2014

Sabine, C. L., Feely, R. A., Gruber, N., Key, R. M., Lee, K., Bullister, J. L., et al. (2004). The oceanic sink for anthropogenic CO_2. *Science*, *305*(5682), 367–371. https://doi.org/10.1126/science.1097403

Séférian, R., Berthet, S., Yool, A., Palmiéri, J., Bopp, L., Tagliabue, A., et al. (2020). Tracking improvement in simulated marine biogeochemistry between CMIP5 and CMIP6. *Current Climate Change Reports*, *6*(3), 95–119. https://doi.org/10.1007/s40641-020-00160-0

Séférian, R., Gehlen, M., Bopp, L., Resplandy, L., Orr, J. C., Marti, O., et al. (2016). Inconsistent strategies to spin up models in CMIP5: Implications for ocean biogeochemical model performance assessment. *Geoscientific Model Development*, *9*(5), 1827–1851. https://doi.org/10.5194/gmd-9-1827-2016

Séférian, R., Nabat, P., Michou, M., Saint-Martin, D., Voldoire, A., Colin, J., et al. (2019). Evaluation of CNRM Earth system model, CNRM-ESM2-1: Role of Earth system processes in present-day and future climate. *Journal of Advances in Modeling Earth Systems*, *11*(12), 4182–4227. https://doi.org/10.1029/2019ms001791

Steinacher, M., Joos, F., Frolicher, T. L., Plattner, G. K., & Doney, S. C. (2009). Imminent ocean acidification in the Arctic projected with the NCAR global coupled carbon cycle-climate model. *Biogeosciences*, *6*(4), 515–533. https://doi.org/10.5194/bg-6-515-2009

Steiner, N. S., Christian, J. R., Six, K. D., Yamamoto, A., & Yamamoto-Kawai, M. (2014). Future ocean acidification in the Canada basin and surrounding Arctic Ocean from CMIP5 Earth system models. *Journal of Geophysical Research: Oceans*, *119*(1), 332–347. https://doi.org/10.1002/2013jc009069

Stock, C. A., Dunne, J. P., Fan, S., Ginoux, P., John, J., Krasting, J. P., et al. (2020). Ocean biogeochemistry in GFDL's Earth System Model 4.1 and its response to increasing atmospheric CO_2. *Journal of Advances in Modeling Earth Systems*, *12*(10). https://doi.org/10.1029/2019ms002043

Tans, P., & Keeling, R. (2023). *Trends in atmospheric carbon dioxide*. NOAA Global Monitoring Laboratory and Scripps Institution of Oceanography.

Taylor, K. E., Stouffer, R. J., & Meehl, G. A. (2012). An overview of CMIP5 and the experiment design. *Bulletin of the American Meteorological Society*, *93*(4), 485–498. https://doi.org/10.1175/bams-d-11-00094.1

Terhaar, J., Frölicher, T. L., Aschwanden, M. T., Friedlingstein, P., & Joos, F. (2022). Adaptive emission reduction approach to reach any global warming target. *Nature Climate Change*, *12*(12), 1136–1142. https://doi.org/10.1038/s41558-022-01537-9

Terhaar, J., Frölicher, T. L., & Joos, F. (2021). Southern Ocean anthropogenic carbon sink constrained by sea surface salinity. *Science Advances*, *7*(18). https://doi.org/10.1126/sciadv.abd5964

Terhaar, J., Frölicher, T. L., & Joos, F. (2022). Observation-constrained estimates of the global ocean carbon sink from Earth System Models. *Biogeosciences*, *19*(18), 4431–4457. https://doi.org/10.5194/bg-19-4431-2022

Terhaar, J., Frölicher, T. L., & Joos, F. (2023). Ocean acidification in emission-driven temperature stabilization scenarios: The role of TCRE and non-CO_2 greenhouse gases. *Environmental Research Letters*, *18*(2), 02403. https://doi.org/10.1088/1748-9326/acaf91

Terhaar, J., Kwiatkowski, L., & Bopp, L. (2020). Emergent constraint on Arctic Ocean Acidification in the twenty-first century. *Nature*, *582*(7812), 379–383. https://doi.org/10.1038/s41586-020-2360-3

Terhaar, J., Orr, J. C., Ethé, C., Regnier, P., & Bopp, L. (2019). Simulated Arctic Ocean response to doubling of riverine carbon and nutrient delivery. *Global Biogeochemical Cycles*, *33*(8), 1048–1070. https://doi.org/10.1029/2019gb006200

Terhaar, J., Orr, J. C., Gehlen, M., Ethé, C., & Bopp, L. (2019). Model constraints on the anthropogenic carbon budget of the Arctic Ocean. *Biogeosciences*, *16*(11), 2343–2367. https://doi.org/10.5194/bg-16-2343-2019

Terhaar, J., Torres, O., Bourgeois, T., & Kwiatkowski, L. (2021). Arctic Ocean acidification over the 21st century co-driven by anthropogenic carbon increases and freshening in the CMIP6 Model Ensemble. *Biogeosciences*, *18*(6), 2221–2240. https://doi.org/10.5194/bg-18-2221-2021

Tjiputra, J. F., Assmann, K., & Heinze, C. (2010). Anthropogenic carbon dynamics in the changing ocean. *Ocean Science*, *6*(3), 605–614. https://doi.org/10.5194/os-6-605-2010

Tjiputra, J. F., Olsen, A., Bopp, L., Lenton, A., Pfeil, B., Roy, T., et al. (2014). Long-term surface pCO_2 trends from observations and Models. *Tellus B: Chemical and Physical Meteorology*, *66*(1), 23083. https://doi.org/10.3402/tellusb.v66.23083

Tokarska, K. B., Stolpe, M. B., Sippel, S., Fischer, E. M., Smith, C. J., Lehner, F., & Knutti, R. (2020). Past warming trend constrains future warming in CMIP6 models. *Science Advances*, *6*(12). https://doi.org/10.1126/sciadv.aaz9549

UNFCC (United Nations / Framework Convention on Climate Change). (2015). *Adoption of the Paris Agreement, 21st Conference of the Parties*. United Nations. AN OFFICIAL PUBLICATION.

Vaittinada Ayar, P., Bopp, L., Christian, J. R., Ilyina, T., Krasting, J. P., Séférian, R., et al. (2022). Contrasting projections of the ENSO-driven CO_2 flux variability in the equatorial Pacific under high-warming scenario. *Earth Syst. Dynam.*, *13*(3), 1097–1118. https://doi.org/10.5194/esd-13-1097-2022

van Vuuren, D. P., Edmonds, J., Kainuma, M., Riahi, K., Thomson, A., Hibbard, K., et al. (2011). The representative concentration pathways: An overview. *Climatic Change*, *109*(1–2), 5–31. https://doi.org/10.1007/s10584-011-0148-z

Völker, C., Wallace, D. W., & Wolf-Gladrow, D. A. (2002). On the role of heat fluxes in the uptake of anthropogenic carbon in the North Atlantic. *Global Biogeochemical Cycles*, *16*(4), 85-1–85-9. https://doi.org/10.1029/2002gb001897

Wang, S., Wang, Q., Wang, M., Lohmann, G., & Qiao, F. (2022). Arctic Ocean freshwater in CMIP6 coupled models. *Earth's Future*, *10*(9). https://doi.org/10.1029/2022ef002878

Weiss, R. F. (1974). Carbon dioxide in water and seawater: The solubility of a non-ideal gas. *Marine Chemistry*, *2*(3), 203–215. https://doi.org/10.1016/0304-4203(74)90015-2

Woosley, R. J., & Millero, F. J. (2020). Freshening of the Western Arctic negates anthropogenic carbon uptake potential. *Limnology & Oceanography*, *65*(8), 1834–1846. https://doi.org/10.1002/lno.11421

Yamamoto, A., Kawamiya, M., Ishida, A., Yamanaka, Y., & Watanabe, S. (2012). Impact of rapid sea-ice reduction in the Arctic Ocean on the rate of ocean acidification. *Biogeosciences*, *9*(6), 2365–2375. https://doi.org/10.5194/bg-9-2365-2012

Zelinka, M. D., Myers, T. A., McCoy, D. T., Po-Chedley, S., Caldwell, P. M., Ceppi, P., et al. (2020). Causes of higher climate sensitivity in CMIP6 models. *Geophysical Research Letters*, *47*(1). https://doi.org/10.1029/2019gl085782

Zika, J. D., Skliris, N., Blaker, A. T., Marsh, R., Nurser, A. J., & Josey, S. A. (2018). Improved estimates of water cycle change from ocean salinity: The key role of Ocean Warming. *Environmental Research Letters*, *13*(7), 074036. https://doi.org/10.1088/1748-9326/aace42

References From the Supporting Information

Boucher, O., Servonnat, J., Albright, A. L., Aumont, O., Balkanski, Y., Bastrikov, V., et al. (2020). Presentation and evaluation of the IPSL-CM6A-LR climate model. *Journal of Advances in Modeling Earth Systems*, *12*(7). https://doi.org/10.1029/2019ms002010

Danabasoglu, G., Lamarque, J. F., Bacmeister, J., Bailey, D. A., DuVivier, A. K., Edwards, J., et al. (2020). The community Earth system model version 2 (CESM2). *Journal of Advances in Modeling Earth Systems*, *12*(2). https://doi.org/10.1029/2019ms001916

Döscher, R., Acosta, M., Alessandri, A., Anthoni, P., Arneth, A., Arsouze, T., et al. (2021). The EC-Earth3 Earth System Model for the Climate Model Intercomparison Project 6. *Geoscientific Model Development Discussions*. https://doi.org/10.5194/gmd-2020-446

Hajima, T., Watanabe, M., Yamamoto, A., Tatebe, H., Noguchi, M. A., Abe, M., et al. (2020). Development of the MIROC-ES2L Earth system model and the evaluation of biogeochemical processes and feedbacks. *Geoscientific Model Development*, *13*(5), 2197–2244. https://doi.org/10.5194/gmd-13-2197-2020

Lovato, T., Peano, D., Butenschön, M., Materia, S., Iovino, D., Scoccimarro, E., et al. (2022). CMIP6 simulations with the CMCC Earth system model (CMCC-ESM2). *Journal of Advances in Modeling Earth Systems*, *14*(3). https://doi.org/10.1029/2021ms002814

Mauritsen, T., Bader, J., Becker, T., Behrens, J., Bittner, M., Brokopf, R., et al. (2019). Developments in the MPI-M Earth System Model Version 1.2 (MPI-ESM1.2) and its response to increasing CO_2. *Journal of Advances in Modeling Earth Systems*, *11*(4), 998–1038. https://doi.org/10.1029/2018ms001400

Seland, Ø., Bentsen, M., Graff, L. S., Olivié, D., Toniazzo, T., Gjermundsen, A., et al. (2020). Overview of the Norwegian Earth System Model (NorESM2) and key climate response of CMIP6 DECK, historical, and scenario simulations. *Geoscientific Model Development*, *13*(12), 6165–6200. https://doi.org/10.5194/gmd-13-6165-2020

Sellar, A. A., Jones, C. G., Mulcahy, J. P., Tang, Y., Yool, A., Wiltshire, A., et al. (2019). UKESM1: Description and evaluation of the U.K. Earth system model. *Journal of Advances in Modeling Earth Systems*, *11*(12), 4513–4558. https://doi.org/10.1029/2019ms001739

Swart, N. C., Cole, J. N., Kharin, V. V., Lazare, M., Scinocca, J. F., Gillett, N. P., et al. (2019). The Canadian Earth System Model Version 5 (CANESM5.0.3). *Geoscientific Model Development*, *12*(11), 4823–4873. https://doi.org/10.5194/gmd-12-4823-2019

Tjiputra, J. F., Schwinger, J., Bentsen, M., Morée, A. L., Gao, S., Bethke, I., et al. (2020). Ocean biogeochemistry in the Norwegian Earth system model version 2 (NORESM2). *Geoscientific Model Development*, *13*(5), 2393–2431. https://doi.org/10.5194/gmd-13-2393-2020

Yukimoto, S., Kawai, H., Koshiro, T., Oshima, N., Yoshida, K., Urakawa, S., et al. (2019). The meteorological research Institute Earth system model version 2.0, MRI-ESM2.0: Description and basic evaluation of the physical component. *Journal of the Meteorological Society of Japan. Ser. II*, *97*(5), 931–965. https://doi.org/10.2151/jmsj.2019-051

Ziehn, T., Chamberlain, M. A., Law, R. M., Lenton, A., Bodman, R. W., Dix, M., et al. (2020). The Australian Earth system model: Access-ESM1.5. *Journal of Southern Hemisphere Earth Systems Science*, *70*(1), 193–214. https://doi.org/10.1071/es19035